Journal of Materials Chemistry C

Accepted Manuscript

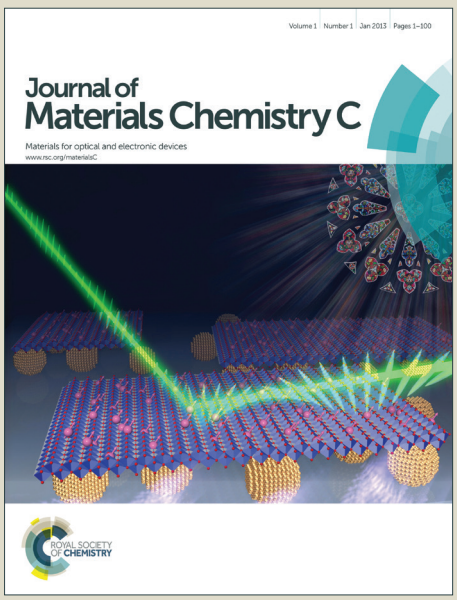

ROYAL SOCIETY OF CHEMISTRY

www.rsc.org/materialsC

Journal Name

ARTICLE

New platinum complexes exhibiting host dependent photoluminescence as single dopant in double emitting layer, voltage independent hybrid white electroluminescence devices

Received 00th January 20xx,
Accepted 00th January 20xx

DOI: 10.1039/x0xx00000x

www.rsc.org/

Anurach Poloek,[abc] Chieh Wang,[ad] Yung-Ting Chang,[a] Chiao-Wen Lin,[a] Chao-Tsen Chen*[c] and Chin-Ti Chen*[ad]

Four heteroleptic platinum complexes (**FPtXND**) bearing 4-hydroxy-1,5-naphthyridine derivatives functionalized with phenyl (**X** = **Ph**), dimethylamino (**X** = **dma**), morpholino (**X** = **mor**), or phenoxazino (**X** = **pxz**) unit as one ligand (**XND**) and 2-(2,4-difluorophenyl)pyridine (**F**) as the other common ligand were newly synthesized and characterized. Each platinum complex has its absorption and photoluminescence (PL) spectroscopic characteristics. With the demonstration from X-ray crystallography (of **FPtdmaND** and **FPtpxzND**), electrochemical and theoretical studies, unusual spectroscopic features of **FPtpxzND**, such as a weak absorption band around 450-600 nm, significant concentration dependent solution PL wavelength but little host dependent thin film PL wavelength (and it is relatively long wavelength), particularly low solution PL quantum yield (Φ_{PL}); relatively strong absorption of **FPtdmaND** and **FPtmorND**; relatively long PL wavelength of **FPtPhND** have acquired reasonable explanation. After each platinum complex being examined for monochromatic organic light-emitting diodes (OLEDs), having relatively high Φ_{PL} as well as appropriate greenish yellow PL of monomeric form) and orange to red PL of aggregate/excimeric form, **FPtdmaND** or **FPtmorND** have been chosen as dopant material in the construction of single or double emitting layer (EML), hybrid white organic light-emitting diodes (OLEDs). High performance warm white electroluminescence (EL) ($CIE_{x,y}$ (0.42-0.43, 0.43-0.44)) was obtained, where the same platinum complex dopant **FPtdmaND** is doped (5 or 8 wt%) in two EMLs, 4,4'-di(9*H*-carbazol-9-yl)-1,1'-biphenyl (CBP) harvesting monomeric emission and highly fluorescent blue *N*,*N*'-di-1-naphthalenyl-*N*,*N*'-diphenyl-[1,1':4',1'':4'',1'''-quaterphenyl]-4,4'''-diamine (4P-NPD) harvesting excimer/aggregate emission. Such warm white EL show high colour rendering index (CRI) of 86-88, reasonably good EL efficiency of 9.7%, 22.5 cd A^{-1}, or 10.7 lm W^{-1}. EL with improved white chromaticity ($CIE_{x,y}$ (0.37-0.39, 0.39-0.41)) can be obtained by using **FPtmorND** as the single dopant, although it has somewhat inferior CRI (84-86) and EL efficiency (8.3%, 20.1 cd A^{-1}, or 9.5 lm W^{-1}). Nevertheless, both double EML, hybrid white OLED exhibit rather constant CRI and $CIE_{x,y}$ under driving voltage between 7 and 10 V.

Introduction

Phosphorescent organic light-emitting diodes (PHOLEDs) have currently attracted extensive attention because of their potential applications in full colour flat-panel displays and solid-state lighting.[1] Owing to strong spin-orbital coupling (SOC) of the heavy metal such as iridium, platinum and osmium, the singlet excitons can be converted into triplet excitons through intersystem crossing (ISC). Theoretically, OLEDs with nearly 100% internal quantum efficiency can be achieved due to harvesting of both singlet (25%) and triplet (75%) excitons.[2] Among these heavy metal complexes,[3,4] platinum complexes are under intensive investigation due to their unique photophysical properties in solid state. Different from that of iridium or osmium complexes, square planar molecular geometry of platinum complex easily promotes molecular aggregation and excimer formation through either a close intermolecular π – π contact or a short metal-metal (Pt-Pt) interaction, which often exhibits red shifted and broadened emission compared with their isolated or non-aggregate form.[5] Thus, platinum complexes have become a popular choice for a single dopant yet exhibiting double emission in the fabricated white OLEDs (WOLEDs), which usually require two or three phosphorescent dopant emitters if they are iridium complexes.[6] The use of platinum complexes as a single dopant in WOLEDs not only facilitates easier fabrication and less costs but also renders high quality lighting application, i.e., high colour rendering index (CRI) ~ 90 due to the broad electroluminescence (EL).

A WOLED based on single phosphorescence dopant can be easily fabricated by coupling sky-blue emission from non-aggregate platinum complex itself and yellow to red emission from its excimer/aggregate.[7-9] For example, Williams *et al*. have reported a sky-blue emitting platinum complex $PtL^{30}Cl$,[8c] which has been used

[a] *Institute of Chemistry, Academia Sinica, Taipei, Taiwan 11529, Republic of China. Email: chintchen@gate.sinica.edu.tw; Fax: +886 2 27831237; Tel: + 886 2 27898542*
[b] *Nano Science and Technology Program, Taiwan International Graduate Program (TIGP), Academia Sinica and National Taiwan University, Taiwan*
[c] *Department of Chemistry, National Taiwan University, Taipei, Taiwan 10617*
[d] *Department of Applied Chemistry, National Chiao Tung University 1001 University Rd., Hsinchu 30050, Taiwan.*

† Electronic Supplementary information(ESI) available: Synthesis, Characterization and device performances. CCDC-1044625 and CCDC-1044626. For ESI and crystallographic data in CIE or other electronic format see DOI: 10.1039/x0xx00000x

as a single dopant for WOLED. Although an EL with a nearly white chromaticity $CIE_{x,y}$ (0.32, 0.37) and a reasonably good CRI of 84 were achieved, the corresponding EL efficiency was low, external quantum efficiency, EQE, and luminous efficiency are 7.1% and 14.3 cd/A, respectively. Similarly, Li *et al*. have reported a perfect white ($CIE_{x,y}$ (0.33, 0.33)) and high efficiencies (EQE ~18% and power efficiency ~35 lm/W) EL based on a single dopant of sky-blue platinum complex Pt-16, although CRI of the device was only 80.[7b] Even though the fabrication of white EL by a single dopant of blue-emitting platinum complex paves the way to simplify the device structure, there are very few true-blue platinum complexes available. In addition, blue phosphorescent dopants still lack of stability and suitable organic host materials with solid-state triplet energy gap > 2.7 eV (phosphorescence wavelength < 460 nm) are relatively limited.

To overcome the instability problem of WOLEDs, which is due to blue phosphorescence dopant emitters, blue fluorescence (F) and yellow/orange/red phosphorescence (P) hybrid is an effective approach to achieve WOLED with long term stability. Moreover, considering the white EL quality (i.e., CRI) and the structure simplicity of WOLED, a single phosphorescence dopant based on non-blue but green-yellow platinum complexes is most beneficial for hybrid WOLED. This is also helpful in lifting restrictions on host material having large triplet energy gap. Surprisingly, there have been just few reports on F-P hybrid WOLED based on single platinum complex dopant.[10] The first successful F-P hybrid, single platinum complex dopant WOLED was demonstrated by Che *et al*.[10a, b] However, the device structure is a bit complicate due to a separated layer of blue fluorescent material (9,10-bis-(*β*-naphthy)-anthrene) in addition to the platinum complex dopant layer. Although high CRI of 88 and good EL efficiencies, EQE over 10%, were achieved, white EL chromaticity of $CIE_{x,y}$ (0.244-0.344, 0.315-0.397) is driving voltage (5.5 to 15.5 V) dependent. With such device structure, it is conceivable that CRI of the white EL is also highly dependent on driving voltages. Later on, Wong *et al*. also presented hybrid WOLEDs having "virtual sunlight" quality EL (CRI as high as 97), of which triphenylgermanium functionalized 2-pheylpyridine platinum complex (Pt-Ge) is the single phosphorescence dopant.[10c] In their devices, hole transporting layer was 4,4'-bis[*N*-(1-naphthyl)-*N*-phenylamino]-biphenyl (NPB) and its weak true-blue emission took part in the hybrid white EL. However, such "virtual sunlight" hybrid WOLEDs had low EL efficiencies (4.1%, 8.3 cd/A, 5.5 lm/W) and both CRI and $CIE_{x,y}$ were also driving voltage dependent. Accordingly, in addition to further simplifying device structure, combining the platinum complex dopant and blue fluorescence material into one layer seems to be feasible for voltage-independent high performance hybrid WOLED. A remained challenge is to find the suitable platinum complex dopant and high efficiency blue fluorescent host.

Recently, we have been the first research group to achieve such hybrid WOLEDs (simple device structure and voltage-independent high performance) by using a highly blue fluorescent host material, *N*,*N*'-di-1-naphthalenyl-*N*,*N*'-diphenyl-[1,1':4',1'':4'',1'''-quaterphenyl]-4,4'''-diamine (4P-NPD),[11] which is doped with a series of heteroleptic platinum complexes bearing 8-subtituted 4-hydroxy-1,5-napthyridine (**ND**) derivatives and 2-(2,4-difluorophenyl)pyridine (F) as two cyclometalated ligands.[12,13] Interestingly, we have shown that the photophysical, electrochemical, and electroluminescent properties can be independently tuned by introducing different substituents on the **ND** ligand. In our continued works to discover more platinum complexes for voltage-independent high performance hybrid WOLEDs, we report here the synthesis, photophysical, theoretical, and electrochemical studies of the influence of the substituent on heteroleptic platinum complexes **FPtXND,** of which **X** denotes phenyl (**Ph**), dimethylamine (**dma**), morpholine (**mor**) or phenoxazine (**pxz**) as the substituent of **ND** ligand (Scheme 1). To test the extended π-conjugation of **ND** ligand and to compare the steric structure effect of aliphatic or aromatic amino donor group of **ND** ligand, we choose **PhND**, **dmaND** (and **morND**), and **pxzND** for platinum complexes and their PL and EL characteristics.

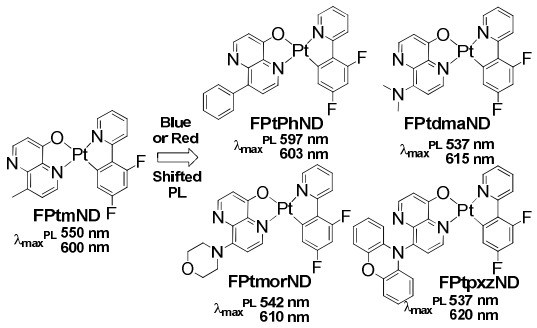

Scheme 1 Chemical structure of **FPtmND** and different **FPtXND**. Two photoluminescence (PL) wavelengths (λ_{max}^{PL}) are included below each platinum complex. The first PL wavelength is based on dilute dichloromethane solution (2 x 10^{-5} M); the second PL wavelength is based on a sample of ~10 wt% in 4P-NPD thin film.

Having different substituents, the electron density distribution of the frontier orbitals of **FPtXND** is altered and the corresponding emission colour can be tuned. Interestingly, in both solution and solid state, these platinum complexes exhibited different PL (Scheme 1). Depending on the host material and the concentration of platinum complex dopant, PL from either monomeric form or excimer/aggregate can be achieved from the thin film containing the platinum complex, of which emission colour ranging from greenish yellow to orange and red, hinging on the substituent of **ND** ligand (see Figure 1). Two different molecular packing patterns obtained from the single crystal X-ray analysis of **FPtdmaND** and **FPtpxzND** illustrate the substituent dependence of emission in solid state. The EL properties of the new platinum complexes have been examined in the common host material 4,4'-di(9*H*-carbazol-9-yl)-1,1'-biphenyl (CBP) showing multi-colour from greenish yellow to orange-red emission. Furthermore, the white ELs of **FPtdmaND** and **FPtmorND** were constructed by utilizing highly blue fluorescent 4P-NPD as the host material together with monomer and aggregate/excimer emission from the platinum complex dopant. With our device designs, unlike previously reported hybrid WOLEDs based on single platinum complex dopant,[10] we are able to separately control the emission of monomeric form and excimer/aggregate by doping platinum complex in CBP and 4P-NPD host materials, respectively.

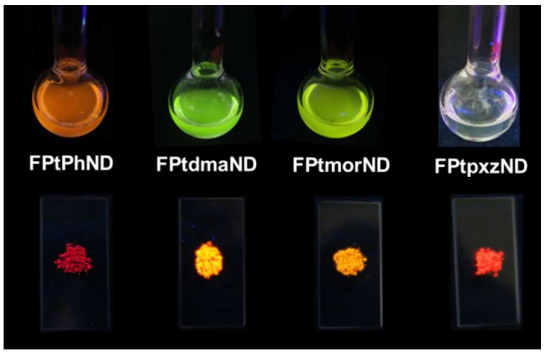

Figure 1 PL image of **FPtPhND**, **FPtdmaND**, **FPtmorND**, and **FPtpxzND** (from the left to right) in degassed diluted dichloromethane solution with $1\sim2 \times 10^{-5}$ M (top row) and as solid powder (bottom row). The solution of **FPtpxzND** exhibits a very weak greenish emission and the bluish appearance is due to the UV lamp; the bright orange emission of **FPtdmaND** powder looks yellowish under the digital camera that we used.

Results and Discussion

Synthesis and Characterisation

The synthesis of ligands and platinum complexes is shown in Scheme 2. The corresponding pyridylamine derivatives as ligand precursors were synthesized according to the literature method (see ESI). The 8-substituted 4-hydroxy-1,5-napthyridine ligands (**XND**) were prepared by Cassis procedure in two steps using Meldrum's acid and pyridylamine derivatives in the first step and followed by intramolecular cyclization in diphenyl ether at 260 °C. This method was previously developed by us.[14]

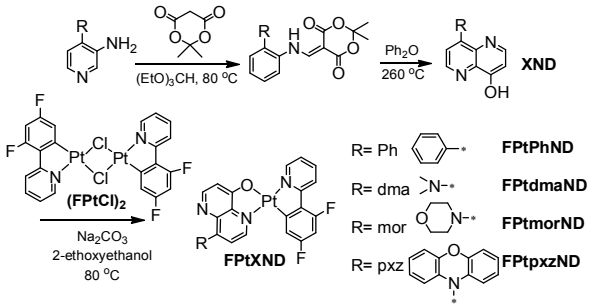

Scheme 2 Synthetic route of 8-substituted 4-hydroxy-1,5-napthyridine ligand (XND) and the platinum complexes FPtXND.

The synthesis of new **FPtXND** follows the previous protocol (Scheme 2),[12] in which Pt μ-dichloro-bridged dimer **$(FPtCl)_2$** was first prepared from K_2PtCl_4 and 2-(2,4-difluorophynyl)pyridine (**F**) in a mixture of 2-ethoxyethanol and water.[15] **$(FPtCl)_2$** was then treated with the **PhND**, **dmaND**, **morND**, and **pxzND** ligands to yield the desired platinum complexes **FPtPhND**, **FPtdmaND**, **FPtmorND**, and **FPtpxzND**, respectively. All of new heteroleptic platinum complexes were confirmed by NMR spectroscopy, mass spectrometry, and elemental analyzes. Moreover, two platinum complexes **FPtdmaND** and **FPtpxzND** were structurally characterized by X-ray crystallography.

X-ray crystallography

Single crystals of **FPtdmaND** and **FPtpxzND** were grown from a dichloromethane/methanol solution. The ORTEP diagrams and some crystal data of **FPtdmaND** and **FPtpxzND** are shown in Figure 2 and 3, respectively.

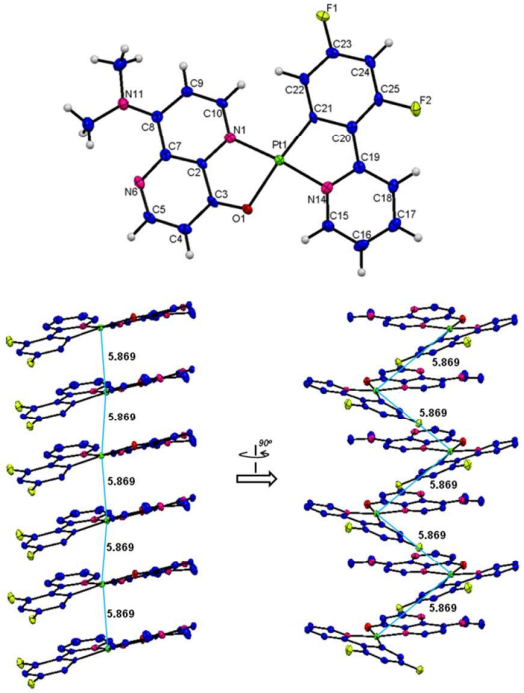

Figure 2 ORTEP diagram of FPtdmaND with thermal ellipsoids shown at the 50% probability level (top). Stacking diagram (from two viewing angle ~90° difference) with an emphasis on the exactly same Pt-Pt distance of 5.87 Å (sky blue line in the bottom). Selected bond lengths (Å): Pt-N(1) = 2.026, Pt-O(1) = 2.078, Pt-N(14) = 1.997, Pt-C(21) = 1.987. In the stacking diagram, all hydrogen atoms are removed for clarity.

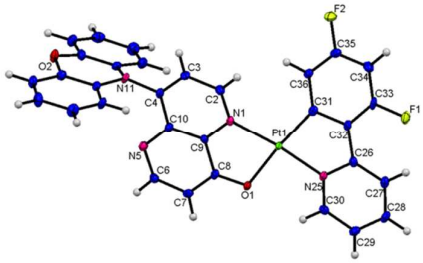

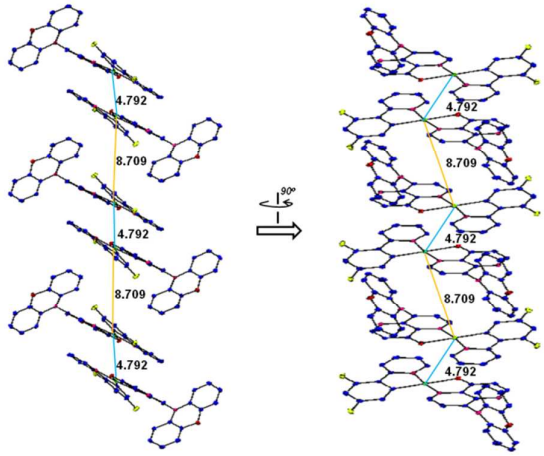

Figure 3 ORTEP diagram of FPtpxzND with thermal ellipsoids shown at the 50% probability level (top). Stacking diagram (from two viewing angle ~90° difference) with an emphasis on the two Pt-Pt distances, 4.79 Å (sky blue lines) and 8.71 Å (golden yellow lines)(bottom). Selected bond lengths (Å): Pt-N(1) = 2.035, Pt-O(1) = 2.092, Pt-N(25) = 1.993, Pt-C(31) = 1.987. In the stacking diagram, all hydrogen atoms and solvent (methanol) molecule are removed for clarity.

Both molecular structures adopt a distorted square planar geometry and reveal *trans* conformation between two coordinating nitrogen atoms of **F** ligand and **ND** ligand. The Pt-N, Pt-C and Pt-O distances of both complexes are similar (see the figure caption of Figure 2 and 3), which are also comparable to those previously reported for **FPtOPhND** and **FPtCzND**, respectively.[12] In addition, the adventitious solvent molecule (methanol) was observed in the crystal lattice of **FPtpxzND**, but it was not found for **FPtdmaND**. Such observation indicates that the molecular packing is more compact for **FPtdmaND** than **FPtpxzND** due to the more steric demanding structure of phenoxazine substituent. Consequently, **FPtdmaND** and **FPtpxzND** display different molecular stacking.

For **FPtdmaND**, as shown in Figure 2, the molecules are arranged in a roughly parallel but sliding side way fashion, having ~56° of crossing angle. From the crystal packing diagram, **FPtdmaND** was found for one single Pt-Pt distance of 5.87 Å, which is significantly longer than those of commonly seen dimeric packing of platinum complex.[17] Such long Pt-Pt distance indicates the absence of Pt-Pt interactions. However, an average short intermolecular π - π distance of 3.57 Å was calculated based on the crystal data, indicative of strong molecular interaction of **FPtdmaND** in solid state. Differently, the molecules of **FPtpxzND** are stacked pairwise in a roughly antiparallel direction (a ~49° was found for the crossing angle) as illustrated in Figure 3. Different to one single Pt-Pt distance found for **FPtdmaND**, **FPtpxzND** has a Pt-Pt distance of 4.79 Å within each stacked pair and a long Pt-Pt distance of 8.71 Å between the adjacent pairs, partially due to the orthogonal configuration (~89° for the dihedral angle) of phenoxazine ring to the molecular plane of **FPtpxzND**. An average intermolecular π - π distance of 3.52 Å was determined from the crystal data. Although relatively long Pt-Pt distances were found for both **FPtdmaND** and **FPtpxzND**, it is the short intermolecular π - π distance of adjacent molecules, resulting different molecular packing that plays an important role for excimer/aggregateformation and photophysical properties in solid state (see PL and EL sections).

UV-visible absorption spectroscopic analysis

The UV-visible absorption spectra of platinum complexes in CH_2Cl_2 at a concentration of $1x10^{-5}$ M are illustrated in Figure 4, and the corresponding data are summarized in Table 1.

All platinum complexes of the series display a strong absorption band peaked around 225-250 nm, which are reasonably assigned to the π-π* local transition (LC) of the coordinated ligands. In the longer wavelength of 300-600 nm, all platinum complexes exhibit multiple and weaker absorption bands with varied absorption intensity, depending on the substituent of the complexes. Particularly, **FPtdmaND** and **FPtmorND** show much stronger absorption band than **FPtPhND** and **FPtpxzND**. This can be attributed to an intraligand charge transfer (ILCT) mixing into singlet metal-to-ligand charge transfer (^{1}MLCT) and triplet metal-to-ligand charge transfer (^{3}MLCT) because of the strong electron-donating nature of amino substituent (i.e. dimethylamine and morpholine).[18] However, a very weak absorption band observed around 475-600 nm (estimated peak ~500 nm and onset ~580 nm) only for **FPtpxzND** is tentatively assigned to a n-π* transition or an ineffective π-π* ILCT due to the aromatic amino substituent phenoxazine and its orthogonal conformation with the naphthyridinolate π-conjugation (see X-ray crystallographic data and the results of theoretical study).

Compared with the previously reported **FPtmND** (λ_{max}^{ab} 415 nm),[11] absorption bands around 400~450 nm of the new platinum complexes are either red-shifted or blue-shifted depending on the electronic nature and the conformation of substituents.[12] Except for **FPtpxzND**, electron-donating substituents of **FPtXND** provide the absorption spectrum a blue-shifting change, such as λ_{max}^{ab} 405 and 407 nm of **FPtdmaND** and **FPtmorND**, respectively. However, a

Table 1 Photophysical data and thermal decomposition temperature of **FPtXND**.

Pt complexes	λ_{max}^{ab} (ε) [nm] in CH_2Cl_2 [10^4 M^{-1} cm^{-1}]	λ_{max}^{PL} [nm] in CH_2Cl_2			Φ_{PL} [a]	τ_p [b] [μs]	T_d [c] [°C]
		$2x10^{-5}$ M	$2x10^{-4}$ M	$2x10^{-3}$ M			
FPtPhND	429 (0.75)	597	601	614	0.22 (0.15)	32.98	313
FPtdmaND	405 (2.44)	537	567	581	0.17 (0.20)	14.45	318
FPtmorND	407 (2.25)	542	570	584	0.23 (0.14)	14.72	357
FPtpxzND	431 (0.58), 500 (0.10)	537	573	632	0.04 (0.04)	4.79	356

[a] PL quantum yields determined in degassed CH_2Cl_2 and 5wt% in PS thin film, respectively.
[b] Room temperature PL lifetime determined in degassed CH_2Cl_2
[c] Thermal decomposition temperature (at 5% weight loss) determined by TGA under nitrogen atmosphere.

red-shifting absorption spectrum (λ_{max}^{ab} 431 nm) is observed for electron-donor substituted **FPtpxzND** and it is ascribed to the orthogonal conformation of phenoxazine substituent, which is virtually not π-conjugated to the naphthyridinolate ligand. Due to the higher electonegativity of nitrogen atom (relative to that of carbon atom) and the π-conjugation lacking orthogonal conformation, aromatic amine phenoxazine substituent of **FPtpxzND** has in fact an electron-withdrawing nature. On the other hand, red-shifting absorption spectrum (λ_{max}^{ab} 429 nm) of **FPtPhND** is because of the phenyl-extended π-conjugation of naphthyridine ligand in LUMO (see electron density contour plot shown in Figure 7). The unusual absorption spectroscopic feature of **FPtpxzND** gets theoretical support from our HOMO/LUMO DFT calculation (see the section of theoretical study). The electron density of HOMO and LUMO or their changes is distinctly different in **FPtpxzND** compared with that of **FPtPhND**, **FPtdmaND**, or **FPtmorND**.

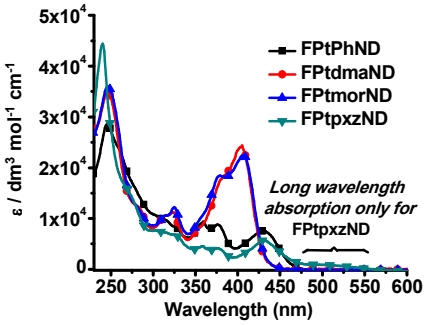

Figure 4 UV-Vis absorption spectra of FPtXND in CH_2Cl_2 at a concentration of $1x10^{-5}$ M.

Photoluminescence spectroscopic analysis

The PL spectra of platinum complexes in solution with varied concentration are illustrated in Figure 5 and corresponding data are summarized in Table 1. In solution with a diluted concentration of 2 x 10^{-5} M, **FPtdmaND**, **FPtmorND**, and **FPtpxzND** exhibit a greenish yellow emission with a peak PL wavelength (λ_{max}^{PL}) at 537, 542 and 537 nm, respectively, whereas an orange emission with λ_{max}^{PL} at 597 nm is observed for **FPtPhND** (see PL images shown in Figure 1).

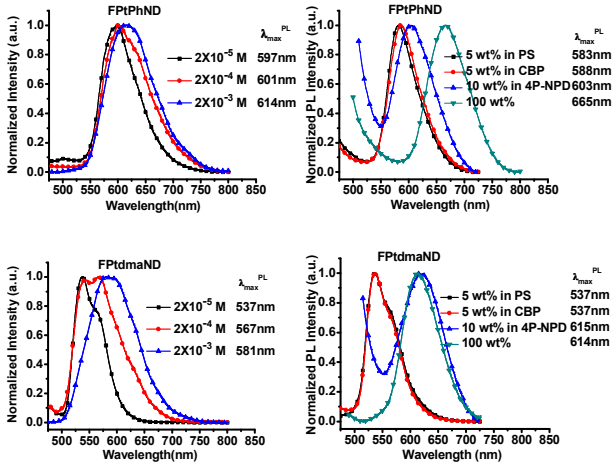

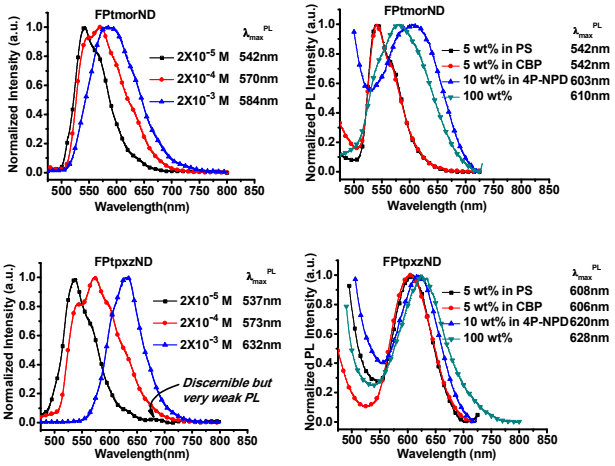

Figure 5 PL spectra of **FPtXND** in CH_2Cl_2 with varied concentrations and in doped thin film with different host materials, PS (5 wt%), CBP (5 wt%), 4P-NPD (10 wt%) and each **FPtXND** (100 wt%).

In diluted solution with concentration of 2 x 10^{-5} M, the emissions can be considered as the PL of non-aggregated platinum complexes (monomers), of which wavelength is mainly determined by the electronic structure or energy level of the molecular orbitals. In general, solution PL wavelength follows the trend of the electron donating strength of the substituent (**FPtdmaND** ~ **FPtmorND** >> **FPtPhND**), where phenyl substituent of **FPtPhND** is not electron donating. Accordingly, a same solution PL wavelength λ_{max}^{PL} 537 nm of **FPtpxzND** and **FPtdmaND** is somewhat puzzling, considering substantially longer absorption wavelength λ_{max}^{ab} 431 nm of **FPtpxzND** than λ_{max}^{ab} 405 nm of **FPtdmaND**. Even excluding the weak absorption around 450-600 nm, **FPtpxzND** has the smallest Stokes shift among four platinum complexes. However, we have noticed a discernible but very weak PL signal around 660-710 nm found only for **FPtpxzND** spectrum (see corresponding solution spectra shown in Figure 5). For energy wise concern, it is quite consistent with the weak and broad absorption around 450-600 nm of **FPtpxzND** (Figure 4 and Figure S4). Trying to understand the unusual absorption (as shown in absorption spectroscopic analysis) and PL spectra of **FPtpxzND**, we have examined the excitation spectra of both **FPtpxzND** and **FPtdmaND** under the same solution concentration ($2x10^{-5}$ M) and at similar PL wavelength of 536/537 nm and 567/573 nm (see Figure 6).

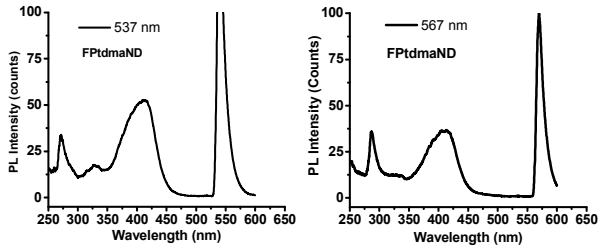

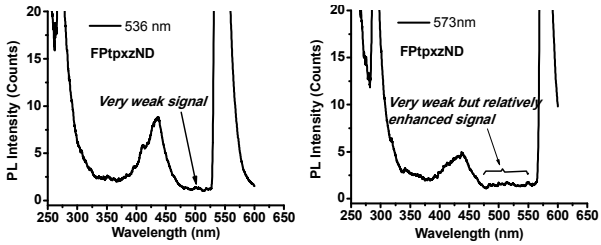

Figure 6 Excitation spectra of **FPtdmaND** and **FPtpxzND** in CH_2Cl_2 with concentration of 2 x10^{-5} M at two wavelengths, 537/535 and 567/573 nm.

From the excitation spectra, we can reassure that the greenish yellow PL (λ_{max}^{PL} 537 nm) of non-aggregate monomeric **FPtdmaND** and **FPtpxzND** mainly originates from the absorption of λ_{max}^{ab} 405 and 437 nm, respectively. Moreover, the spectrum around 450-550 nm is relatively enhanced in 573 nm PL detection spectrum of **FPtpxzND**, indicating the very weak 650-710 nm PL is probably due to the 450-600 nm absorption. Such spectroscopic feature was only found for **FPtpxzND** not for **FPtdmaND** or **FPtmND**, of which excitation spectra are shown in Figure S2. Therefore, phenoxazine substituent has a distintive influence on the spectroscopic characteristics of **FPtXND.** Finally, since there is a great spectroscopic intensity difference between excitation spectra of **FPtdmaND** and **FPtpxzND**, we can anticipate that solution PL quantum yield (Φ_{PL}) of **FPtpxzND** is significantly smaller than that of **FPtdmaND**.

Closely relevant to the molecular interaction, four platinum complexes all exhibit red-shifting solution PL spectra when the concentration of solution increases from 2x10^{-5} to 2x10^{-3} M (see Figure 5 left column), although the red-shifting PL is found most pronounced for **FPtpxzND**. These red-shifted solution PL spectra taken place at higher concentrations can be considered as more PL contribution from the aggregates/excimers of the platinum complexes, which basically arise from either π-π stacking from their aromatic ligands or Pt-Pt contact in short distance rendering metal-metal-to-ligand charge transfer transition (MMLCT) excited state in solution. Some platinum complexes are known to show low-energy PL from MMLCT state. [18]

In 5 or 10 wt% doped thin film of polystyrene (PS) or CBP, except for **FPtpxzND**, all platinum complexes exhibit PL spectra very similar to those of diluted solution (see Figure 5 right column). **FPtpxzND** is different from the other three platinum complexes regarding its red-shifted PL spectra of doped PS or CBP, showing λ_{max}^{PL} at 606 nm. When switching the thin film host material to 4P-NPD, **FPtPhND**, **FPtdmaND**, and **FPtmorND** display significant red-shifted and broadened spectra, which are similar to those of platinum complex neat film (spectra marked with 100 wt% in Figure 5). **FPtpxzND** is also different from the rest platinum complexes in terms of limitedly red-shifting spectra of doped 4P-NPD or neat thin film. On the other hand, PL λ_{max}^{PL} of doped 4P-NPD and neat thin film are similar for **FPtdmaND** and **FPtpxzND**, but they are quite different for **FPtPhND** and **FPtmorND** (see Figure 5 right column).

Qualitatively, in addition to the different solid state solvation power (molecular interaction between host and dopant) of different thin film host materials (PS, CBP, and 4P-NPD), different molecular packing in solid state, which we have witnessed from the X-ray crystal structures of **FPtdmaND** and **FPtpxzND**, plays an important role of the solid state PL wavelength. Different from the uniformly column-like packing of **FPtdmaND** molecule, **FPtpxzND** has a pair-wise molecular packing in solid state and such packing is tighter because of a shorter π–π (plane-to-plane) distance and a shorter Pt-Pt distance as well compared with those of **FPtdmaND** (see their X-ray crystallographic analysis). The distinctive PL spectroscopic feature of **FPtpxzND** in solution or in doped thin film can be correlated to its molecular structure that is decisive for molecular interaction in concentrated solution or in doped thin film. In doped thin film, both **FPtPhND** and **FPtpxzND** show only orange to red colour PL regardless in which host material. Lacking greenish yellow emission, they are not suitable for composing high quality hybrid white EL with blue fluorescent 4P-NPD. Accordingly, **FPtdmaND** or **FPtmorND** will be a better choice for the fabrication of hybrid white OLEDs.

The Φ_{PL} of solution and doped PS thin film are summarized in Table 1. In diluted solution of CH_2Cl_2, the platinum complexes display Φ_{PL} of 22%, 17%, 23% and 4% for **FPtPhND**, **FPtdmaND**, **FPtmorND** and **FPtpxzND**, respectively. The PL Φ_{PL} of 5 wt% **FPtXND** in the PS thin film are 15%, 20%, 14% and 4% for **FPtPhND**, **FPtdmaND**, **FPtmorND** and **FPtpxzND**, respectively. It is notable that **FPtdmaND** has the highest Φ_{PL} in the PS thin film among all platinum complexes. Therefore, in terms of doped thin film PL Φ_{PL}, **FPtdmaND** is expected to be our best phosphorescence material in the fabrication of both monochromatic and hybrid white OLEDs. In addition, the PL lifetimes (τ) of **FPtXND** were also determined in a diluted solution of CH_2Cl_2. Four new platinum complexes have τ of 32.98, 14.45, 14.72 and 4.79 μs for **FPtPhND**, **FPtdmaND**, **FPtmorND**, and **FPtpxzND**, respectively (see decay profile in Figure S3 and data in Table 1). These platinum complexes have the emission lifetime in the microsecond regime, implying the phosphorescence nature of the emission. Notably, a relatively long emission lifetime of 32.98 μs was determined for **FPtPhND** and it can be ascribed to the low lying ^{3}LC involved in the emission process,[19] which is in turn due to the more extended π-conjugation of **PhND** ligand. ^{3}LC is mostly organic ligand based and not much heavy metal (Pt) involved. Therefore, it is relatively long lived compared with ^{3}MLCT state. On the other hand, the relatively short τ of 4.79 μs observed for **FPtpxzND** may be attributed to the quenching effect from the non-conjugated phenoxazine substituent. Such quenching effect (probably caused by a photoinduced electron transfer from phenoxazine moiety) may explain a very low PL Φ_P 4% observed for **FPtpxzND**.

Thermal properties

The thermogravimetric analysis (TGA) of new platinum complexes data are shown in Figure 7 and Table 1. The newly synthesized heteroleptic platinum complexes, **FPtPhND**, **FPtdmaND**, **FPtmorND** and **FPtpxzND** exhibited relatively high thermal stabilities with the decomposition temperature (T_d, corresponding to 5% weight loss) at 313, 318, 357, and 356 °C, respectively. Owning to their high thermal stabilities, all new platinum complexes are acceptable to use in OLED fabrication by vacuum-thermal-deposition process.

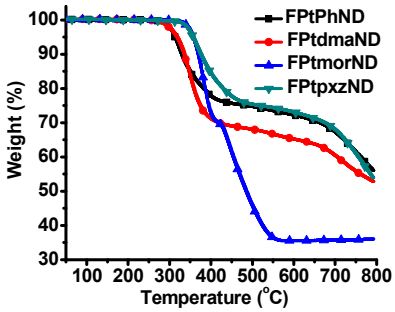

Figure 7 Thermogravicmetric analysis (TGA) data of FPtXND.

Theoretical studies

To gain insight into the electronic effect of substituents on the platinum complexes, quantum chemical calculations were performed using DFT with the hybrid B3LYP functional and 6-31G* basis set. The results are shown in Figure 8. **FPtPhND** exhibited very similar electron density of HOMO and LUMO to those previously reported **FPtmND** and **FPtmmND**.[12] The HOMO electron density are mostly found on the pyridinolate part of phenylnaphthyridinolate (**PhND**), difluorophenyl moiety, and platinum metal ion, whereas the LUMO electron density are largely located on **PhND** ligand and the pyridine ring of **F** ligand. We have noticed that there is an extension of LUMO electron density on the phenyl substituent of **ND** ligand, which may be the cause of longer absorption and emission wavelength of **FPtPhND** than that of **FPtdmaND** or **FPtmorND**. Different from that of **PhND**, strong electron donating substituent of dimethylaminonaphthyridinolate (**dmaND**) or morpholinonaphthyridinolate (**morND**) increases the HOMO electron density on dimethylamine or morpholine substituted **ND** ligand. On the other hand, both amino substituents significantly reduce the LUMO electron density of whole **ND** ligand, compared with that of **FPtPhND**. On that basis calculation, the lowest energy electronic transition mainly arises from ligand-based local charge transfer (LC) and some mixed ^{1}MLCT and ^{3}MLCT. In general, LC has a stronger absorption intensity than that of ^{1}MLCT or ^{3}MLCT. Although they all have amine substituent, the distribution of HOMO electron density of **FPtpxzND** is totally different from that of **FPtdmaND** or **FPtmorND** (see Figure 8). Nearly all HOMO electron density of **FPtpxzND** concentrates on phenoxazine substituent, trace electron density found on **ND** ligand itself, and nothing on difluorophenyl moiety or platinum metal ion. Unlike the local π-π* transition of π-conjugated **PhND** ligand, π-conjugation is virtually impossible between phenoxazine substituent and **ND** ligand because of orthogonal conformation between these two π-conjugation moieties. Therefore, DFT calculation qualitatively verifies our previous n-π* transition or an ineffective π-π* ILCT assignment of the weak absorption band around 475-600 nm of **FPtpxzND**.

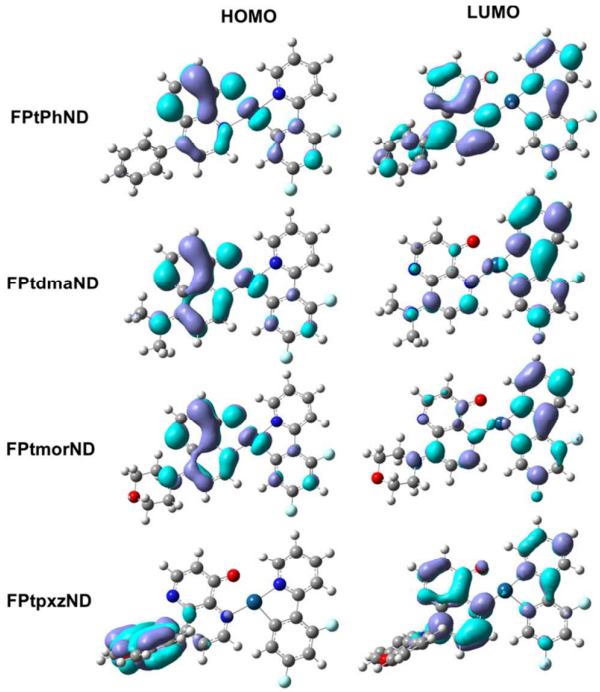

Figure 8 Calculated electron density contour plots of HOMO (left) and LUMO (right) of **FPtXND**.

Electrochemical properties and the estimation of HOMO-LUMO energy level

The electrochemical behaviors of the platinum complexes were investigated in CH_2Cl_2 by cyclic voltammetry (CV) as shown in Figure 9. The details of CV data are listed in Table 2. The energy level of HOMO of each platinum complex was determined from the first electrochemical oxidation potential (*vs*. saturated $Ag/AgNO_3$). Here, due to the ill-profile of most platinum complexes, we took the anodic peak of each cyclic voltammogram as the first oxidation potential in the calculation of HOMO energy level. Except for **FPtpxzND**, the first electrochemical oxidation takes place on **ND** ligand, particularly around pyridinolate platinum (II) part of the molecule. Electron-rich substituent, such as diamehtylamine or morpholine, of **ND** ligand will reduce the oxidation potential of the molecule like that of **FPtdmaND** or **FPtmorND**. The phenyl substituent of **FPtPhND** is not electron donating, resulting the highest oxidation potential (0.77 V) among the series. **FPtpxzND** is unusual in terms of its first oxidation potential of 0.67 V, which is substantially higher than 0.56 and 0.60 V of **FPtdmaND** and

Table 2 Electrochemical data of **FPtXND**

Pt Complexes	$E^{oxd,1}$ (V)	E_{HOMO} (eV)	λ_{onset} (nm)[a]	E_g (eV)[b]	E_{LUMO} (eV)[c]
FPtPhND	0.77	5.32	470	2.64	2.68
FPtdmaND	0.56	5.11	432	2.87	2.24
FPtmorND	0.60	5.15	437	2.84	2.31
FPtpxzND	0.67	5.22	580	2.14	3.08
ferrocene	0.25	—	—	—	—

[a] Determined from the onset wavelength of absorption spectrum. [b] Estimated from the onset absorption spectrum by equation of $E_g = 1240/\lambda_{onset}$. [c] Deduced from the E_{HOMO} and E_g.

FPtmorND. All of these three platinum complexes have a substituent that is electron-donating amine. Unlike that of **FPtPhND**, **FPtdmaND** or **FPtmorND**, it is reasonable to surmise that the first electrochemical oxidation process of **FPtpxzND** occurs on phenoxazine substituent instead of napthyridinolate platinum (II) part of the molecule. Such inference is consistent with the distribution of HOMO electron density estimated from our theoretical study (see Figure 8). It is also in accordance with a fact that **FPtpxzND** is the only exception that all platinum complexes exhibit ill-profile of cyclic voltammograms (see Figure 9). In addition to the spectroscopic properties shown earlier, the special electrochemical feature of **FPtpxzND** can be attributed to its orthogonal conformation between phenoxazine substituent and the naphthyridinolate moiety.

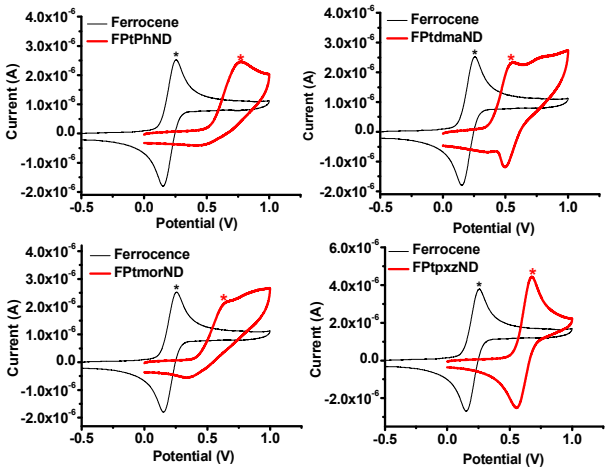

Figure 9 Cyclic voltammograms of **FPtdmaND**, **FPtmorND**, **FPtpxzND**, **FPtPhND**, and ferrocene reference.

Based on the onset wavelength of the absorption spectra in diluted solution (1 x 10^{-5} M) (Figure S4), **FPtdmaND** and **FPtmorND** having an electron-donating substituent displayed a larger energy gaps (E_g) and hence a higher lying LUMO energy level than that of **FPtPhND**. Due to the long wavelength (450~600 nm) absorption band of n-π^* transition or an ineffective π-π^* ILCT, **FPtpxzND** has a relatively small E_g and low lying LUMO energy level. The HOMO and LUMO energy levels of other materials including 4,4'-bis[N-(1-naphthyl)-N-phenylamino]-biphenyl (NPB), 4P-NPD, CBP and 1,3,5-tris(N-phenylbenzimidazole-2-yl)benzene (TPBI) were estimated similarly and their energy levels are aligned in Figure 10. From the HOMO energy level alignment between the host materials, CBP or 4P-NPD, and **FPtXND** dopants, most of EL energy will be confined on the **FPtXND** dopants if CBP used as the host material. It will not be the case if 4P-NPD used as the host material. Some of the EL energy will be the blue fluorescence of 4P-NPD host. This is a desired situation in achieving hybrid white light-emitting.

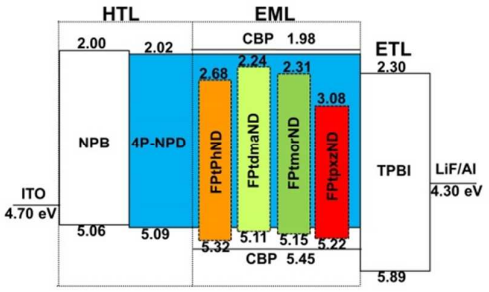

Figure 10 Energy level alignment of materials involved in hybrid WOLEDs. Colour code of each phosphorescent dopant is based on $CIE_{x,y}$ chromaticity of Device A and B.

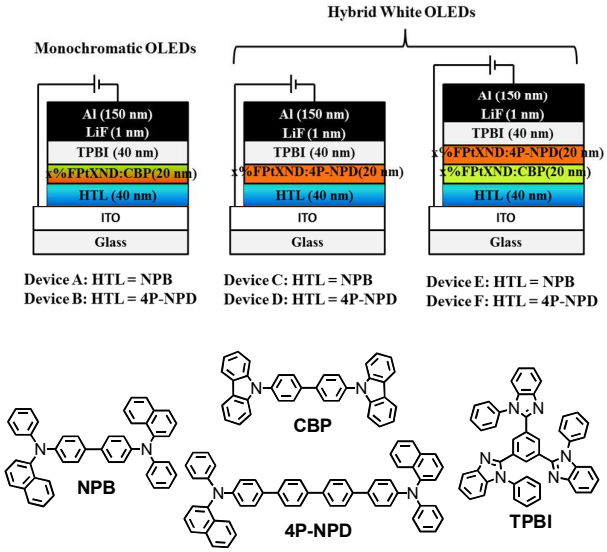

Figure 11 The device configurations and the molecular structures of the relevant compounds used in these devices.

Electroluminescence properties

Monochromatic OLEDs

To evaluate the monochromatic EL properties of new platinum complexes, PHOLEDs were fabricated using **FPtPhND**, **FPtdmaND**, **FPtmorND**, and **FPtpxzND** as emitters. The monochromatic OLEDs in this work were constructed by vacuum-thermal-deposition process. Two different materials, NPB and 4P-NPD, were employed as hole-transporting layers (HTL) in Device A and B, respectively. The device structure used for Device A and B was ITO/NPB or 4P-NPD (40nm)/CBP: *x*% **FPtXND** (20 nm)/TPBI (40nm)/LiF (1 nm)/Al (150 nm) as shown in Figure 11, in which CBP was used as host material, whereas TPBI was used as electron-transporting layer (ETL). The device performances were optimized by varying the dopant concentration of **FPtXND**, i.e., *x* = 2, 5, or 8 wt%. The EL spectra and device performance data of Device A and B are shown in Figure 12, Figure S5, and Table 3.

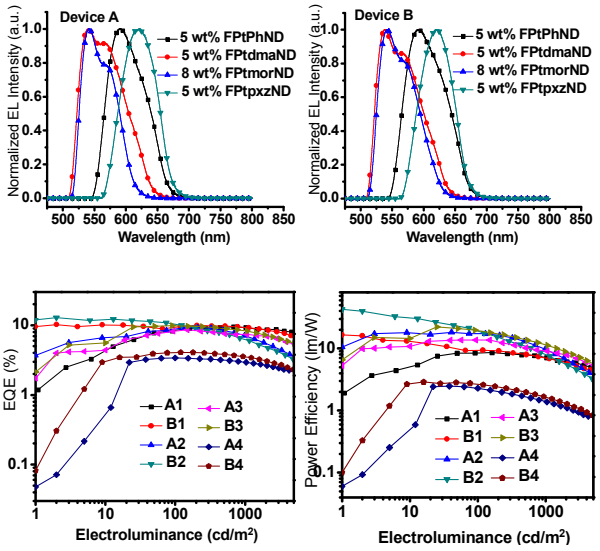

Figure 12 Normalized EL spectra of Device A and B with optimized dopant concentrations of platinum complexes (top); electroluminance dependent external quantum efficiency (EQE) of Device A and B (bottom).

Having CBP as the host material, devices mainly exhibited monochromatic colour, either greenish yellow or orange-red, from different platinum complex dopants. Regardless different material of HTL, both Device A and B exhibited similar EL spectra, although device performances of Device B are in general better than those of Device A. We attribute such EL performance to the superior hole mobility of 4P-NPD than NPB as previously reported.[21] A greenish yellow phosphorescence EL was obtained with **FPtdmaND** or **FPtmorND** in all dopant concentrations, 2, 5, and 8 wt%. Nonetheless, with increasing dopant concentration, EL spectra become broadened, suggestive of aggregate/excimer formation. The optimized device performances data of different platinum complexes dopants are summarized in Table 3.

Whereas it was 5 wt% for **FPtdmaND** (Device A2 and B2), 8 wt% was found the optimum dopant concentration for **FPtmorND** (Device A3 and B3). The EL spectra of both platinum dopants are similar to the PL spectra of the corresponding platinum complexes in a diluted solution. Device A2 and B2 (**FPtdmaND** dopant devices) are the most efficient greenish yellow devices, giving $CIE_{x,y}$ (0.42-0.43, 0.56-0.57) with the peak EL efficiency of 9.3%, 36.2 cd A^{-1}, or 18.3 lm W^{-1} and 12.2%, 50.9 cd A^{-1}, or 40.0 lm W^{-1}, respectively. The high EL efficiency of **FPtdmaND** may be attributed to its high Φ_{PL} of 20% (in PS thin film), the highest among four platinum complexes. Whereas the orange EL with $CIE_{x,y}$ (0.58-0.59, 0.41) was achieved by employing **FPtPhND** as dopant. The best EL efficiency of **FPtPhND** devices was obtained at dopant concentration of 5 wt% and it is 9.5%, 24.5 cd A^{-1}, or 8.6 lm W^{-1} for Device A1 and 10.2%, 25.4 cd A^{-1}, or 16.0 lm W^{-1} for Device B1. Differently, upon employing **FPtpxzND** as dopant emitter, EL spectra (λ_{max}^{EL} around 617-623 nm) in all dopant concentration are red-shifted compared with the PL spectra of diluted solution. However, such EL spectra are similar to the PL spectra of concentrated solution and doped thin film with PS, CBP or 4P-NPD as the host material. We may reasonably assume that **FPtpxzND** tends to aggregate more readily than the other three platinum complexes regardless the nature of host material. The best red EL efficiencies obtained for **FPtpxzND** is 5 wt% one with EL efficiency of 3.4%, 5.8 cd A^{-1}, or 2.5 lm W^{-1} for Device A4 and 4.1%, 7.1 cd A^{-1}, or 2.9 lm W^{-1} for Device B4. Although the red devices exhibited a relatively low EL efficiency due to its low Φ_{PL} of 4% (in PS thin film), the $CIE_{x,y}$ (0.65, 0.35) of both Device A4 and B4 is close to $CIE_{x,y}$ (0.67, 0.33), the standard red chromaticity of National Television Standards Committee.[22]

Table 3 Device performances with different doping concentrations.

Device	Dopant	Dopant Conc. (wt%)	λ_{max}^{EL} (nm)	V_{on} (V)[a]	EQE (%)[b]	CE (cd A^{-1})[b]	PE (lm W^{-1})[b]	L,Voltage (cd m^{-2}) (V)[c]	CIE (x,y)[d]	CRI[e]
A1	**FPtPhND**	5	590	5.0	9.4(9.5)	24.3(24.5)	7.8(8.6)	9869(15)	(0.58,0.41)	-
B1	**FPtPhND**	5	592	4.5	9.8(10.2)	24.2(25.4)	13.4(16.0)	9627(15)	(0.59,0.41)	-
A2	**FPtdmaND**	5	540	3.5	8.6(9.3)	32.9(36.2)	13.0(18.3)	13846(15)	(0.43,0.56)	-
B2	**FPtdmaND**	5	538	3.5	7.8(12.2)	30.2(50.9)	30.5(40.0)	11650(15)	(0.42,0.57)	-
A3	**FPtmorND**	8	542	4.0	7.6(8.6)	32.5(36.8)	10.2(13.7)	10892(15)	(0.39,0.60)	-
B3	**FPtmorND**	8	542	4.0	9.0(9.9)	37.1(40.8)	13.9(22.3)	14159(15)	(0.41,0.58)	-
A4	**FPtpxzND**	5	622	4.5	3.2(3.4)	5.4(5.8)	1.7(2.5)	4247(15)	(0.65,0.35)	-
B4	**FPtpxzND**	5	620	4.5	3.8 (4.1)	6.6(7.1)	2.0(2.9)	4889(15)	(0.65,0.35)	-
C1	**FPtdmaND**	8	458,626	5.0	4.6(6.4)	6.0(8.4)	1.8(3.3)	2266(15)	(0.36,0.27)	62
D1	**FPtdmaND**	8	455,634	5.0	5.1(7.0)	6.7(9.2)	1.9(3.5)	2663(15)	(0.37,0.28)	64
C2	**FPtmorND**	8	456,630	4.5	4.5(4.6)	5.8(5.9)	1.9(2.0)	4136(15)	(0.30,0.23)	50
D2	**FPtmorND**	8	456,629	4.5	3.4(5.1)	4.4(6.5)	1.6(3.1)	4038(15)	(0.32,0.23)	55
E1	**FPtdmaND**	5 & 8	455,540,576	4.5	6.0(9.0)	13.6(20.7)	5.3(9.7)	5139(15)	(0.44,0.45)	84
F1	**FPtdmaND**	5 & 8	454,540,574	4.5	8.4(9.7)	18.9(22.5)	6.0(10.7)	6468(15)	(0.43,0.44)	86
E2	**FPtmorND**	8 & 8	456,542,573	5.0	6.0(7.6)	15.1(18.7)	4.9(9.0)	4900(15)	(0.38,0.41)	80
F2	**FPtmorND**	8 & 8	456,542,578	4.5	7.5(8.3)	17.9(20.1)	5.9(9.5)	5452(15)	(0.39,0.41)	84

[a] Turn-on voltage is the one at which the luminance over 1 cd m^{-2} was obtained. [b] The data for external quantum efficiency (EQE), current efficiency (CE), and power efficiency (PE) obtained at 500 cd/m^2. The data of peak efficiency is listed in parentheses of efficiency data. [c] Maxmium electroluminance and driving voltage. [d] Commission Internationale d'Eclairage chromaticity coordinates at 7~9 V; [e] Colour rendering index at 7~9 V.

F-P Hybrid WOLEDs

To investigate the hybrid white OLEDs, **FPtdmaND** and **FPtmorND** are selected due to their high Φ_{PL} and greenish yellow PL and orange-red PL in CBP and 4P-NPD thin film, respectively. To achieve the hybrid white EL, a blue fluorescent 4P-NPD was used as the host material for the platinum complex dopants. Thus, simple device structures of Device C and D with single emitting layer (EML) were first fabricated (see Figure 10). Except for EML, Device C and D basically have similar architectures to the aforementioned monochromatic devices (Device A and B) and they are ITO/NPB or 4P-NPD (40nm)/ 4P-NPD: *x*% **FPtXND** (20 nm)/TPBI (40nm)/LiF(1 nm)/Al (150 nm), of which the dopant concentration (x%) was also tried 2, 5, and 8 wt%. White or near white EL spectra of Device C and D are shown in Figure 13; corresponding device performances are summarized in Figure 14 and Table 3. Both platinum complex dopants showed the white EL at 8 wt% dopant concentration. Once again, whenever employing 4P-NPD as HTL, both Device C and D exhibited better EL performances On the other hand, devices having **FPtdmaND** as the dopant (Device C1 and D1) outperform devices having **FPtmorND** as the dopant (Device C2 and D2). This is probably due to the more contribution of orange-red phosphorescence EL from **FPtdmaND** than **FPtmorND** (see Figure 13). Higher EL efficiencies of Device C1 and D1 may be also due to the higher Φ_{PL} of **FPtdmaND** than **FPtmorND** in doped PS thin film (Table 3). The best white EL efficiency of 7.0%, 9.2 cd A^{-1}, or 3.5 lm W^{-1} were obtained from Device D1 with $CIE_{x,y}$ (0.37,0.28) and CRI of 64. Although the hybrid white OLEDs having similar device configuration exhibit better EL efficiency by using **FPtdmaND** than previously reported **FPtmND**, **FPtmmND** and **FPtppND**, Device C1 and D1 have significantly lower CRI of 62-64 (lower than CRI of 80~85). Due to the more red-shifted aggregate/excimeric **FPtdmaND** EL (λ_{max}^{EL} around 626-634 nm) as compared to those previously reported **FPtmND**, **FPtmmND** and **FPtppND** EL (λ_{max}^{EL} around 581-614 nm), there is a less coverage of visible spectrum and hence lower CRI. Due to the similar reason, red-shifted EL spectra, Device C2 and D2 have dissatisfied CRI of 50 and 55, respectively, which are even worse than those of Device C1 and D1. However, the weaker orange-red EL contribution from **FPtmorND** aggregate/excimer is the additional cause of low CRI herein.

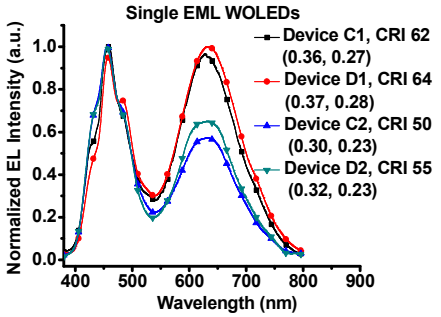

Figure 13 Normalized hybrid white EL spectra of single EML device (Device C and D) with 8 wt% **FptdmaND** or **FptmorND** dopant concentration.

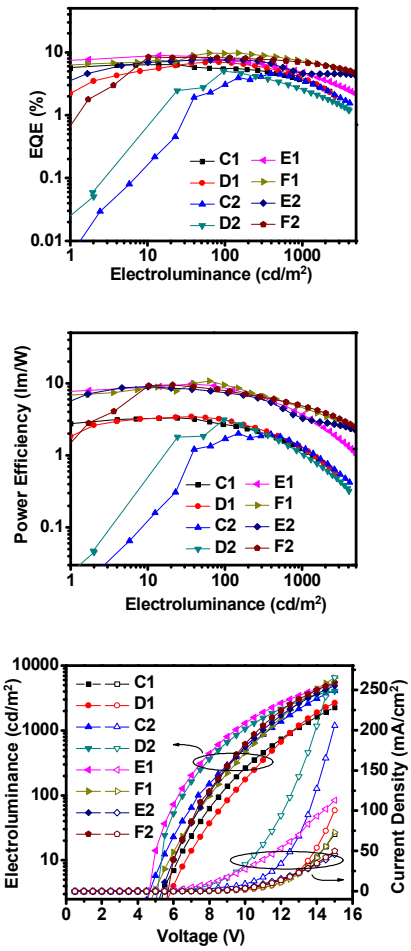

Figure 14 External quantum efficiency and power efficiency as a function of electroluminance of hybrid white Device C, D, E and F (top and centre figures); their electroluminance-voltage-current density curves (bottom figure).

In order to improve EL quality (CRI) as well as EL efficiency of hybrid white OLED, greenish yellow EL from the monomer of platinum complex is required in filling up the spectroscopic gap between blue and orange-red emission. Therefore, one more EML using CBP as the host material was inserted before 4P-NPD hosted EML. The new device structures (Device E and F shown in Figure 10) were constructed as ITO/NPB or 4P-NPD (40nm)/CBP: *x*% **FPtXND** (20 nm)/4P-NPD: *x*% **FPtXND** (20 nm)/TPBI (40nm)/LiF(1 nm)/Al (150 nm). The dopant concentrations of platinum complexes in CBP and 4P-NPD EMLs were controlled at 5 and 8 wt% for **FPtdmaND** devices and 8 and 8 wt% for **FPtmorND** devices. The EL spectra are illustrated in Figure 15; corresponding device performances are summarized in Figure 14 and Table 3.

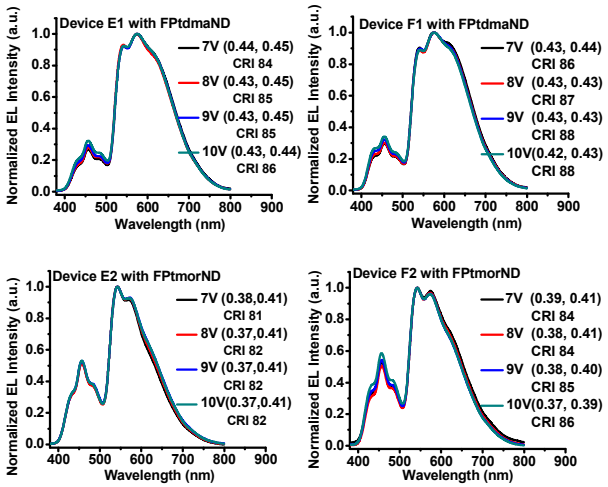

Figure 15 Normalized hybrid white EL spectra of double EML devices (Device E and F) with varied driving voltage of 7, 8, 9, and10 V.

Regardless which dopant material, either **FPtdmaND** or **FPtmorND**, the EL spectra of Device E and F are now dominated by both monomeric and aggregate/excimeric emissions from platinum complexes. Compared with that of Device C and D (Figure 13), blue ELs of Device E and F are all relatively weaker and this can be mainly attributed to the additional phosphorescence emitting layer of the device (x% FPtXND:CBP), which is responsible for the partial replacement of light-emitting that takes place on blue fluorescent 4P-NPD in Device C or D. As a result, the green-yellow-orange-red EL produces much boarder spectra than those of single EML devices (Device C and D), resulting in significantly better white EL efficiency and CRI. Device E and F produced the white ELs with $CIE_{x,y}$ (0.37-0.44, 0.39-0.45) and high CRI of 81- 88. Moreover, the white EL of Device E and F shows slight variation under different driving voltage from 7 to 10 V (see Figure 15). Virtually no voltage dependence of $CIE_{x,y}$, and CRI may be attributed to the effective charge confinement within the double EML structure of Device E and F, which is in turn due to the appropriate alignment of the energy levels of HTL, ETL, the host and dopant materials of EML.

Among double EML devices, Device F1 (**FPtdmaND** dopant and 4P-NPD HTL) displays the best EL performance with the peak EL efficiency of 9.7%, 22.5 cd A^{-1}, or 10.7 lm W^{-1} and satisfied CRI of 86-88. However, Device E1 and F1 exhibit in fact a warm white EL, showing $CIE_{x,y}$ (0.42-0.44, 0.43-0.45) because blue fluorescence contribution from 4P-NPD host is substantially reduced as compared to its single EML device (see EL spectra of Device C1 and D1 in Figure 12). For double EML **FPtmorND** devices, Device E2 and F2 show inferior device performances to Device E1 and F1. Comparing white EL spectra in Figure 15, the green-yellow-orange-red emission band of Device E2 or F2 is somewhat narrower, which is due to a smaller orange-red contribution from aggregate/excimer of **FPtmorND**. Moreover, both devices exhibit more blue fluorescence contribution from 4P-NPD host than Device E1 or F1. As a result, Device E2 or F2 showed better white chromaticity with $CIE_{x,y}$ (0.37-0.39, 0.39-0.41), although CRI of 80 and 84 is worse than 84 and 86 of Device E1 and F1, respectively. Notably, at 10 V, Device F2 displayed white EL colour with $CIE_{x,y}$ (0.37,0.39), which is pretty close to standard white EL as $CIE_{x,y}$(0.33,0.33). Nonetheless, due to the smaller phosphorescence-based EL contribution of **FPtmorND** as mentioned above, the EL efficiencies of Device E2 and F2 (**FPtmorND** dopant devices) are not as good as those of Device E1 and F1 (**FPtdmaND** dopant devices).

Conclusions

We have reported four newly synthesized platinum complexes, **FPtXNDs**. Their PL spectroscopic characteristics have been carefully studied both in solution with various concentration and in doped thin film with different host materials. With electrochemical, theoretical, and X-ray crystallographic studies, we have demonstrated and rationalized the varied aggregate/excimeric PL observed for each **FPtXNDs**, of which different substituent on the ND ligand has a profound influence on either solution or thin film PL. Based on the greenish yellow PL in CBP hosed thin film, orange red PL in 4P-NPD hosed thin film, and PL quantum yield in doped PS thin film, **FPtdmaND** and **FPtmorND** are chosen to fabricate high performance hybrid white OLEDs as a single dopant in single or double EML configuration devices. In double EML devices with a combination of the current **FPtdmaND** or **FPtmorND** dopant as well as CBP and the blue fluorescent 4P-NPD as the host materials, high performance hybrid white OLEDs are achieved: reasonably good EL efficiencies, 9.7%, 22.5 cd A^{-1}, and 10.7 lm W^{-1} for **FPtdmaND** and 8.3%, 20.1 cd A^{-1}, and 9.5 lm W^{-1} for **FPtmorND**; high CRI of 84~88. Significantly, the hybrid white OLEDs studied here exhibit little variation on $CIE_{x,y}$ and CRI between 7-10 V of device driving voltage. This is a beneficial feature in the WOLED lighting application. However, through this study, we have found a compromising result between white colour chromaticity, i.e., $CIE_{x,y}$, and EL efficiency. Such problem may be overcome by other high performance blue fluorescent host materials, which are the materials being looked after extensively now.

Experimental Section

General information

Photoluminescence (PL) spectra were recorded on a Hitachi fluorescence spectrophotometer F-4500, and the same spectrophotometer was used to record the EL spectra of OLEDs. UV-visible electronic absorption spectra were recorded on a Hewlett-Packard 8453 Diode Array spectrophotometer. The ^{1}H and ^{13}C NMR spectra were recorded on a Bruker AMX-400 MHz, AVA-400 MHz or Bruker AV-500 MHz Fourier-transform spectrometer at room temperature. Elemental analyses (on a Perkin-Elmer 2400 CHN Elemental Analyser) and electrospray ionization (ESI) or matrix-assisted laser desorption/ionization time-of-flight (MALDI-TOF) mass spectra (on a VA Analytical 11-250J or 4800 MALDI TOF/TOF Analyser) were recorded by the Elemental Analyses and Mass Spectroscopic Laboratory in-house service of the Institute of Chemistry, Academic Sinica. Thermogravimetric analyse was performed under nitrogen with a Perkin-Elmer TGA-7 TG analyser.

Luminescence lifetime was determined on an Edinburgh FL920 time-correlated pulsed single-photon-counting instrument. The phosphorescence emission was detected at 90° via a second Czerny-Turner design monochromator onto a thermoelectrically cooled red-sensitive photomultiplier tube. The resulting photon counts were stored on a microprocessor based multichannel analyzer. The instrument response function was profiled using a scatter solution and subsequently deconvoluted from the emission data to yield an undisturbed decay. Nonlinear least squares fitting of the PL decay curves were performed with the Levenburg-Marquardt algorithm and implemented by the Edinburgh Instruments F900 software.

Solution (in degassed CH_2Cl_2) PL Φ_{PL} was determined with $[Ru(bpy)_3](PF_6)_2$ (bpy = 2,2′-bipyridine) in acetonitrile as a reference (Φ_{PL} = 0.062)[23] and calculated according to the following equation: $\Phi_s = \Phi_r(B_r/B_s)(n_s/n_r)^2(D_s/D_r)$, where the subscripts *s* and *r* refer to sample and reference standard solution respectively, *n* is the refractive index of the solvents, *D* is the integrated intensity, and Φ is the luminescence quantum yield. The quantity *B* was calculated by $B = 1 - 10^{-AL}$, where A is the absorbance at the excitation wavelength and L is the optical path length. The solid-state (PS thin film) PL quantum yields of the platinum complexes were determined by the integrating-sphere method.[24,25]

Redox potentials of the compounds were determined by cyclic voltammetry (CV) using a BAS 100B electrochemical analyzer with a scanning rate at 100 mV/s. The interested compounds were dissolved in deoxygenated dry CH_2Cl_2 with 0.1 M tetrabutylammonium perchlorate as the electrolyte. We used a platinum working electrode and a saturated nonaqueous $Ag/AgNO_3$ referenced electrode. Ferrocene was used for potential calibration (all reported potentials are referenced against Ag/Ag+) and for reversibility criteria. Energy level of ferrocene (4.8 V below the vacuum level) is used as the reference.[26] The HOMO energy levels were calculated with empirical relation $E_{HOMO} = -e[(E^{oxd,1} - E_{(ferrocene)}) + 4.8]$ eV. Due to the ill-profile of the first oxidation potential, we took the relative peak position of anodic current of ferrocene and **FPtXND** cyclic voltammograms in the calculation of HOMO energy level.

X-ray Crytallography studies

Data collection was carried out on a Brucker X8APEX CCD diffractometer at 100 K for **FPtdmaND** and **FPtpxzND** single crystals. The radiation of Mo radiation (λ = 0.71073 Å) was used for both crystals. The unit cell parameters were obtained by a least-square fit to the automatically centered settings for reflections. Intensity data were collected by using the $\omega/2\theta$ scan mode. Corrections were made for Lorentz and polarization effects. The structures were solved by direct methods *SHELX-97*.[27] All non-hydrogen atoms were located from the difference Fourier maps and were refined by full-matrix least-squares procedures. The position of hydrogen atoms was calculated and located. Calculations and full-matrix least-squares refinements were performed utilizing the *WINGX* program package[28] in the evaluation of values of R (F_o) for reflections with I > 2σ(I) and R_w (F_o), where $R = \sum||F_o| - |F_c||/\sum|F_o|$ and $R_w = [\sum\{w(F_o^2 - F_c^2)^2\}/\sum\{w(F_o^2)^2\}]^{1/2}$. Intensities were corrected for absorption.

OLED device fabrication and measurements

OLED devices were fabricated by thermal vacuum deposition. The substrate was an indium-tin-oxide (ITO) coated glass (Merck Display Technology, Taiwan) with a sheet resistance of < 30 Ω/sq. ITO-coated glass substrates were cleaned with detergent, deionized water, acetone, and isopropanol, followed by oxygen plasma treatment. The current density–voltage–luminance characteristics of the devices were measured using a Keithley 2400 source meter and a Newport 1835C optical meter equipped with a Newport 818-ST silicon photodiode, respectively. The device was placed close to the photodiode such that all the forward light entered the photodiode. The effective size of the emitting diodes was 4.00 mm^2, which is significantly smaller than the active area of the photodiode detector, a condition known as "under-fillling", satisfying the measurement protocol.[29] This is one of the most conventional ways in measuring the EL efficiency of OLEDs, although sometimes experimental errors may arise due to the non-Lambertian emission of OLEDs. The colour rendering index (CRI) of white OLEDs was measured by a spectroradiometer (Specbos 1201, JETI Technishe Instrumente GmbH).

Materials

For the materials used in device fabrication, NPB,[30] CBP,[31] TPBI,[32] 2-(2,4-difluorophenyl)pyridine (**F**)[33] and 4P-NPD[11] were prepared via published methods. All materials were purified by vacuum train sublimation before the usage in device fabrication. Synthetic precursors for pyridylamine derivatives were prepared by adopting the synthetic protocols reported in literatures with slight modification as shown in ESI. The Pt μ-dichloro-bridged dimer **$(FPtCl)_2$** was prepared following literature procedures.[34] All reactions were performed under nitrogen. Solvents were carefully dried and distilled from appropriate drying agents prior to use. The syntheses of ligands and platinum complexes are summarized in Scheme 2. The detailed procedure and structural characterization data of the new compounds are shown below.

General synthesis procedure of pre-XND

To a mixture of 4-substituted pyridine-3-amine derivatives (1 equivalent) and Meldrum's acid 2,2-dimethyl-[1,3]dioxane-4,6-dione (1.2 equivalent) was added triethyl orthoformate (6 equivalent). The mixture was then heated at reflux under nitrogen for 4 h. After cooling to room temperature, the reaction solution was evaporated under reduced pressure. The resulting solid was purified by flash column chromatography (silica gel, ethyl acetate/dichloromethane: 1/1) to afford **pre-XND**.

5-((4-phenylpyridin-3-ylamino)methylene)-2,2 dimethyl-1,3-dioxane-4,6-dione (pre-PhND). The specific amounts of chemicals used: 4-phenylpyridin-3-amine (3.00 g, 17.63 mmol), Meldrum's acid (3.05 g, 21.15 mmol) and triethyl orthoformate(15.70 g, 105.75 mmol). The product (**pre-PhND**) was obtained as a pale yellow solid (4.79 g, 84%). ^{1}H NMR (400 MHz, $CDCl_3$): δ 11.35 (d, 1H, *J* = 13.6 Hz), 8.77 (s, 1H), 8.68 (s, 1H), 8.64 (s, 1H), 8.58 (d, 1H, *J* = 4.8 Hz), 7.60-7.53 (m, 3H), 7.41 (d, 1H, *J* = 8.0 Hz), 7.34 (d, 1H, *J* = 4.8 Hz), 1.70 (s, 6H). ^{13}C NMR (100 MHz, $CDCl_3$): δ 165.14, 163.05, 152.72, 147.84,

140.86, 139.33, 133.93, 132.28, 129.75, 129.61, 128.54, 124.84, 105.21, 88.77, 27.08. EI-MS : calcd. 324.1, *m/z* = 324.1 (M^+).

5-((4-(dimethylamino)pyridin-3-ylamino)methylene)-2,2-dimethyl-1,3-dioxane-4,6-dione (pre-dmaND). The specific amounts of chemicals used: N^4,N^4-dimethylpyridine-3,4-diamine (**3a**) (5.00 g, 36.47 mmol), Meldrum's acid (6.30 g, 43.74 mmol) and triethyl orthoformate (19.85 g, 133.94 mmol). The product (**pre-dmaND**) was obtained as a white solid (2.74 g, 37%). ^{1}H NMR (400 MHz, $CDCl_3$): δ 11.45 (d, 1H, *J* = 15.6 Hz), 8.77 (d, 1H, *J* = 15.6 Hz), 8.60 (s, 1H), 8.44(d, 1H, *J* = 5.2 Hz), 7.03 (d, 1H, *J* = 5.2 Hz), 3.95 (t, 4H, *J* = 4.8 Hz), 3.01 (t, 4H, *J* = 4.8 Hz), 1.77 (s,6H). ^{13}C NMR (100 MHz, $CDCl_3$): δ 165.38, 163.08, 151.24, 149.71, 148.69, 138.66, 128.77, 114.71, 105.24, 88.38, 66.56, 51.00, 27.05. FAB-MS: calcd. 291.1, *m/z* = 292.1 ($M+H^+$).

5-((4-morpholinopyridin-3-ylamino)methylene)-2,2-dimethyl-1,3-dioxane-4,6-dione (pre-morND). The specific amounts of chemicals used: 4-morpholinopyridin-3-amine (4.00 g, 22.33 mmol), Meldrum's acid (3.86 g, 26.78 mmol) and triethyl orthoformate (19.85 g, 133.94 mmol). The product (**pre-morND**) was obtained as a white solid (2.74 g, 37%). ^{1}H NMR (400 MHz, $CDCl_3$): δ 11.45 (d, 1H, *J* = 15.6 Hz), 8.77 (d, 1H, *J* = 15.6 Hz), 8.60 (s, 1H), 8.44(d, 1H, *J* = 5.2 Hz), 7.03 (d, 1H, *J* = 5.2 Hz), 3.95 (t, 4H, *J* = 4.8 Hz), 3.01 (t, 4H, *J* = 4.8 Hz), 1.77 (s, 6H). ^{13}C NMR (100 MHz, $CDCl_3$): δ 165.38, 163.08, 151.24, 149.71, 148.69, 138.66, 128.77, 114.71, 105.24, 88.38, 66.56, 51.00, 27.05. EI-MS: calcd. 333.1, *m/z* = 333.2 ($M+H^+$).

5-((4-(10H-phenoxazin-10-yl)pyridin-3-ylamino)methylene)-2,2-dimethyl-1,3-dioxane-4,6-dione (pre-pxzND). The specific amounts of chemicals used: 4-(10H-phenoxazin-10-yl)pyridin-3-amine (1.00 g, 3.63 mmol), Meldrum's acid (0.63 g, 4.37 mmol) and triethyl orthoformate (3.23 g, 21.79 mmol). The product (**pre-pxzND**) was obtained as a white solid (1.38 g, 86%). ^{1}H NMR (400 MHz, $CDCl_3$): δ 11.53 (d, 1H, J = 13.6Hz), 8.74 (d, 1H, *J* = 4.8 Hz), 8.68 (d, 1H, *J* = 13.6Hz), 7.51 (d, 1H, *J* = 5.2 Hz), 6.84-6.77 (m, 4H), 6.68-6.64 (m, 2H), 5.90 (d, 2H, *J* = 8.4 Hz), 1.67 (s, 6H). ^{13}C NMR (100 MHz, $CDCl_3$) δ 165.11, 163.11, 151.75, 149.74, 144.53, 140.77, 137.29, 134.82, 131.21, 126.88, 123.80, 123.71, 116.93, 112.92, 105.68. EI-MS : calcd. 429.1, *m/z* = 429.1 (M^+).

General synthesis procedure of XND ligands

Compound **pre-XND** (1~2 g) in diphenyl ether (35 mL) was heated at 260 °C and stirred under nitrogen atmosphere for 10-60 min. During the reaction, the colour of the solution changed from orange yellow to dark brown or black. After cooling to room temperature, the reaction solution was filtered to isolate solid product. The solid was rinsed with diphenyl ether and subjected to purification by zone-temperature sublimation.

4-Hydroxy-8-phenyl-1,5-naphthyridine (PhND). The specific amounts of chemicals used: **pre-PhND** (1.00 g, 3.08 mmol). The product was obtained as a white solid (0.49 g, 77%). ^{1}H NMR (400 MHz, CD_3OD): δ 8.77 (d, 1H, *J* = 4.4 Hz), 7.91 (d, 1H, *J* = 7.6 Hz), 7.65-7.55 (m, 6H), 6.54 (d, 1H, *J* = 7.6 Hz). ^{13}C NMR (100 MHz, CD_3OD): δ 179.78, 148.16, 143.19, 142.13, 141.89, 136.21, 135.74, 130.95, 130.77, 130.28, 128.50, 112.54. EI-MS: calcd. 222.1, *m/z* = 222.1 (M^+).

4-Hydroxy-8-dimethylamino-1,5-naphthyridine (dmaND). The specific amounts of chemicals used: **pre-dmaND** (5.00 g, 17.18 mmol). The product was obtained as a white solid (2.29 g, 70%). ^{1}H NMR (400 MHz, CD_3OD): δ 8.25 (s, 1H), 8.14 (d, 1H, *J* = 5.6 Hz), 7.00 (s, 1H), 6.59 (d, 1H, *J* = 5.6 Hz), 3.31 (s, 6H). ^{13}C NMR (100 MHz, CD_3OD): δ 172.23, 157.01, 146.46, 141.93, 137.79, 135.55, 113.07, 108.92, 44.26. FAB-MS: calcd. 189.1, *m/z* = 190.1 ($M+H^+$).

4-Hydroxy-8-morpholino-1,5-naphthyridine (morND). The specific amounts of chemicals used: **pre-morND** (2.50 g, 7.50 mmol). The product was obtained as a pale yellow solid (0.98 g, 57%). ^{1}H NMR (400 MHz, CD_3OD): δ 8.49 (s, 1H), 7.98 (d, 1H, *J* = 6.8 Hz), 7.29 (s, 1H), 6.48 (d, 1H, *J* = 6.8 Hz), 3.91 (t, 4H, *J*= 4.8 Hz), 3.24 (t, 4H, *J* = 4.8 Hz). ^{13}C NMR (100 MHz, CD_3OD): δ 178.65, 174.91, 148.02, 142.63, 141.13, 140.74, 134.21, 115.85, 112.78, 67.71, 52.96. EI-MS: calcd. 231.1, *m/z* = 231.1 (M^+).

4-Hydroxy-8-(10H-phenoxazin-10-yl)-1,5-naphthyridine (pxzND). The specific amounts of chemicals used: **pre-pxzND** (1.00 g, 2.33 mmol). The product was obtained as a brown solid (0.50 g, 68%). ^{1}H NMR(400 MHz, CD_3OD) : δ 8.96 (d, 1H, *J* = 4.8 Hz), 7.90 (d, 1H, *J* = 7.2 Hz), 7.87 (d, 1H, *J* = 4.8 Hz), 6.81-6.74 (m, 4H), 6.66-6.62 (m, 2H), 6.57 (d, 1H, *J* = 7.2 Hz), 5.85 (dd, 2H, *J* = 8.0 Hz, *J* = 1.2 Hz). ^{13}C NMR (125 MHz, CD_3OD): δ 180.02, 150.15, 145.61, 144.18, 142.01, 139.55, 137.86, 133.50, 130.98, 130.67124.95, 124.08, 119.95, 117.20, 116.82, 114.29, 113.76. EI-MS: calcd. 327.1, *m/z* = 327.1 (M^+).

General procedure for synthesis of FPtXND complexes

The Pt complex **$(FPtCl)_2$** were prepared following literature procedures.[15] The K_2PtCl_4 and 2.5 equivalent of **F** ligand were mixed in a 3:1 mixture of 2-ethoxyethanol and water. The mixture was heated to 80 °C for 16 h. The desired **$(FPtCl)_2$** were precipitated in the water. The resulting yellow-greenish powder was filtered and was subsequently reacted with **XND** ligand without further purification. A stirred mixture of **$(FPtCl)_2$** (1 equivalent), Na_2CO_3 (10 equivalent) and **XND** ligand (2.1 equivalent) in 2-ethoxyethanol was heated to 80 °C for 16 h. After cooling, the solution was concentrated under reduced pressure. The resultant residue was subjected to column chromatography (silica gel, CH_2Cl_2/MeOH 15:1(v/v)) to afford product.

FPtPhND. The specific amounts of chemicals used: **$(FPtCl)_2$** (0.083 g, 0.38 mmol), Na_2CO_3 (0.190 g, 1.80 mmol) and **PhND** (0.188 g, 1.77 mmol). The product was obtained as a yellow solid (0.069 g, 32%). ^{1}H NMR (400 MHz, $CDCl_3$): δ 9.26 (d,1H, *J* = 5.6 Hz) 8.93 (d, 1H, *J* = 5.6 Hz), 8.55 (d, 1H, *J* = 5.6 Hz), 7.99-7.85 (m, 4H), 7.64 (d, 1H, *J* = 5.6 Hz), 7.59-7.53 (m, 3H), 7.16 (t, 1H, *J* = 5.6 Hz), 6.95 (d, 1H, *J* = 7.2 Hz), 6.84 (d, 1H, *J* = 5.2 Hz), 6.63 (td, 1H, *J* = 7.2 Hz, *J* = 1.6 Hz). ^{13}C NMR (100 MHz, CD_3Cl): δ 163.91, 154.20, 151.31, 149.71, 145.21, 139.62, 130.57, 129.84, 128.79, 124.26, 122.34, 122.14, 121.80, 114.70, 114.50, 112.60, 100.10, 99.84, 99.58. HR-MALDI-MS: calcd. 606.08, *m/z* = 607.09 ($M+H^+$). Anal. Found (calcd) for $C_{25}H_{15}F_2N_3OPt$: C 49.45(49.51), H 2.71 (2.49), N 6.77 (6.93).

FPtdmaND. The specific amounts of chemicals used: **$(FPtCl)_2$** (0.150 g, 0.18 mmol), Na_2CO_3 (0.188 g, 1.80 mmol) and **dmaND** (0.071 g, 0.38 mmol). The product was obtained as an orange-red solid (0.190 g, 76%). ^{1}H NMR (400 MHz, CD_3Cl): δ 9.41 (d, 1H, *J* = 6.0 Hz), 8.57 (d, 1H, *J* = 6.4 Hz), 8.32 (d, 1H, *J* = 5.2 Hz), 8.05 (d, 1H, *J* = 8.4 Hz), 7.90 (t, 1H, *J* = 7.8 Hz), 7.21 (t, 1H, *J* = 6.2 Hz), 7.07 (dd, 1H, *J* = 9.4 Hz), 6.88 (d, 1H, *J* = 5.6 Hz), 6.66-6.61 (m, 2H), 3.59 (s, 6H). ^{13}C

NMR (100 MHz, $CDCl_3$): δ 173.37, 163.77, 155.00, 149.49, 148.97, 146.09, 143.47, 138.98, 122.28, 122.09, 121.70, 114.83, 114.64, 112.22, 105.11, 99.51, 99.28, 99.01, 43.57. HR-MALDI-MS: calcd. 573.09, *m/z* = 573.09 (M^+). Anal. Found (calcd) for $C_{21}H_{16}F_2N_4OPt$: C 43.90 (43.98), H 2.77 (2.81), N 9.40 (9.77).

FPtmorND. The specific amounts of chemicals used: **$(FPtCl)_2$** (0.150 g, 0.18 mmol), Na_2CO_3 (0.188 g, 1.80 mmol) and **morND** (0.087 g, 0.38 mmol). The product was obtained as a yellow solid (0.090 g, 41%). ^{1}H NMR (400 MHz, $CDCl_3$): δ 9.35 (d, 1H, *J* = 5.2 Hz), 8.65 (d,1H, *J* = 6.4 Hz), 8.33 (d, 1H, *J* = 5.2 Hz), 8.03 (d, 1H, *J* = 8.0 Hz), 7.89 (t, 1H, *J* = 8.0 Hz), 7.21 (dd, 1H, *J* = 5.2 Hz), 7.01 (d, 1H, *J* = 8.8 Hz), 6.86 (d, 1H, *J* = 5.2 Hz), 6.79 (d, 1H, *J* = 6.0 Hz), 6.65 (t, 1H, *J* = 9.8 Hz), 4.03 (s, 4H) 4.00 (s, 4H). ^{13}C NMR (100 MHz, CD_3Cl): δ 163.79, 155.66, 149.97, 149.57, 146.56, 139.25, 122.34, 122.17, 121.77, 114.75, 112.48, 107.22, 99.53. HR-MALDI-MS: calcd. 615.11, *m/z* = 615.10 (M^+). Anal. Found (calcd) for $C_{23}H_{18}F_2N_4O_2Pt$: C 44.82 (44.88), H 2.90 (2.95), N 8.99 (9.10).

FPtpxzND. The specific amounts of chemicals used: **$(FPtCl)_2$** (0.150 g, 0.18 mmol), Na_2CO_3 (0.190 g, 1.80 mmol) and **pxzND** (0.122 g, 0.38 mmol). The product was obtained as an orange solid (0.055 g, 22%). ^{1}H NMR (400 MHz, $CDCl_3$): δ 9.42 (d,1H, *J* = 4.4 Hz), 9.23 (d, 1H, *J* = 5.6 Hz), 8.56 (d, 1H, *J* = 5.6 Hz), 8.13 (d, 1H, *J* = 8.8 Hz), 7.98 (t, 1H, *J* = 7.8 Hz), 7.87 (d, 1H, *J* = 5.6 Hz), 7.31 (t, 1H, *J* = 6.4 Hz), 7.07 (dd, 1H, *J* = 9.2 Hz), 6.97 (d, 1H, *J* = 5.6 Hz), 6.79 (dd, 2H, *J* = 7.6 Hz), 6.74 (t, 3H, *J* = 7.4 Hz), 6.60 (td, 2H, *J* = 7.6 Hz), 5.96 (d, 2H, *J* = 8.0 Hz). ^{13}C NMR (100 MHz, CD_3Cl): δ 149.89, 147.82, 144.36, 144.08, 132.82, 127.16, 123.48, 122.82, 122.58, 122.38, 122.04, 116.32, 114.80, 114.33, 113.75, 100.51, 100.25. HR-MALDI-MS: calcd. 711.11, *m/z* = 712.11 ($M+H^+$). Anal. Found (calcd) for $C_{31}H_{18}F_2N_4O_2Pt$: C 52.34 (52.33), H 2.40 (2.55), N 7.74 (7.87).

Acknowledgements

We thank the Ministry of Science and Technology (NSC 101-2113-M-001-004-MY2), Taiwan International Graduate Program (TIGP) of Academia Sinica, Academia Sinica, and National Taiwan University for financial support.

References

1 (*a*) M A. Baldo, M. E. Thomson and S. R. Forrest, *Nature*, 2000, **403**, 750; (*b*) B. W. D' Andrade and S. R. Forrest, *Adv. Mater.*, 2004, **16**, 1585; (*c*) S. Chen, L. Deng, J. Xie, L. Xie, Q. Fan and W. Huang, *Adv. Mater.*, 2010, **22**, 5227; (*d*) H. Sasabe and J. Kido, *Chem. Mater.*, 2011, **23**, 621; (*e*) K. S. Yook and J. Y. Lee, *Adv. Mater.*, 2012, **24**, 3169; (*f*) Y. L. Chang, B. A. Kamino, Z. Wang, M. G. Helander, Y. Rao, L. Chai, S. Wang, T. P. Bender and Z. H. Lu, *Adv. Funct. Mater.*, 2013, **23**, 3204.

2 (*a*) M. A. Baldo, D. F. Brien, Y. You, A. Shoustikov, S. Sibley and M. E. Thompson, *Nature*, 1998, **395**, 151; (*b*) B. Tong, Q. Mei, S. Wang, Y. Fang, Y. Meng and B. Wang, *J. Mater. Chem.*, 2008, **18**, 1636; (*c*) L. Xiao, Z. Chen, B. Qu, J. Luo, S. Kong, Q. Gong and J. Kido, *Adv. Mater.*, 2011, **23**, 926; (*d*) W. C. H. Choy, W. K. Chan and Y. Yuan, *Adv. Mater.*, 2014, **26**, 5368.

3 (*a*) C.-M. Che, C.-C. Kwok, S.-W. Lai, A. F. Rausch, W. J. Finkenzeller, N. Zhu and H. Yersin, *Chem. Eur. J.*, 2010, **16**, 233; (*b*) Z. M. Hudson, C. Sun, M.G. Helander, H. Amarne, Z.-H. Lu and S. Wang, *Adv. Funct. Mater.*, 2010, **20**, 3426; (*c*) A. Y.-Y. Tam, D. P.-K. Tsang, M.-Y. Chan, N. Zhu and V. W.-W. Yam, *Chem. Commun.*, 2011, **47**, 3383; (*d*) S. C. F. Kui, F.-F. Hung, S.-L. Lai, M.-Y. Yuen, C.-C. Kwok, K.-H. Low, S. S.-Y. Chui and C.-M. Che, *Chem. Eur. J.*, 2012, **18**, 96; (*e*) Z. M. Hundson, C. Sun, M.G. Helander, Y.-L. Chang, Z.-H. Lu and S. Wang, *J. Am. Chem. Soc.*, 2012, **134**, 13930.

4 (*a*) E. S.-H. Lam, D. P.-K. Tsang, W. H. Lam, A. Y.-Y. Tam, M.-Y. Chan, W.-T. Wong and V. W.-W. Yam, *Chem. Eur. J.*, 2013, **19**, 6385; (*b*) G. Cheng, P.-K. Chow, S. C. F. Kui, C.-C. Kwok and C.-M. Che, *Adv. Mater.*, 2013, **25**, 6765; (*c*) C. Cebrián, M. Mauro, D. Kourkoulos, P. Mercandlli, D. Hertel, K. Meerholz, C. A. Strassert and L. D. Cola, *Adv. Mater.*, 2013, **25**, 437; (*d*) F. Nisic, A. Colombo, C. Dragonetti, D. Roberto, A. Valore, J. M. Malick, M. Cocchi, G. R. Freemane and J. A. G. Williams, *J. Mater. Chem. C*, 2014, **2**, 1791; (*e*) X. Wang, Y.-L. Chang, J.-S. Lu, T. Zhang, Z.-H. Lu and S. Wang, *Adv. Funct. Mater.*, 2014, **24**, 1911; (*f*) Y. Li, D. P.-K. Tsang, C. K.-M. Chan, K. M.-C. Wong, M.-Y. Chan and V. W.-W. Yam, *Chem. Eur. J.*, 2014, **20**, 13710.

5 (*a*) E. Rossi, L. Murphy, P. L. Brothwood, A. Colombo, C. Dragonetti, D. Roberto, R. Ugo, M. Cocchi and J. A. G. Williams, *J. Mater. Chem.*, 2011, **21**, 15501; (*b*) K. M.-C. Wong and V. W.-W. Yam, *Acc. Chem. Res.*, 2011, **44**, 424; (*c*) E. Rossi, A. Colombo, C. Dragonetti, D. Roberto, F. Demartin, M. Cocchi, P. Brulatti, V. Fattorie and J. A. G. Williams, *Chem. Commun.*, 2012, **48**, 3182; (*d*) D. Kourkoulos, C. Karakus, D. Hertel, R. Alle, S. Schmeding, J. Hummel, N. Risch, E. Holder and K. Meerholz, *Dalton Trans.*, 2013, **42,** 13612; (*e*) T. Shigehiro, S. Yagi, T. Maeda, H. Nakazumi, H. Fujiwara and Y. Sakura, *J. Phys. Chem. C*, 2013, **117**, 532.

6 (*a*) Q. Wang and D. Ma, *Chem. Soc. Rev.*, 2010, **39**, 2387; (*b*) M. C. Gather, A. Köhnen and K. Meerholz, *Adv. Mater.*, 2011, **23**, 233.

7 (*a*) X. Yang, Z. Wang, S. Madakuni, J. Li and C. E. Jabbour, *Appl. Phys. Lett.*, 2008, **93**, 193305; (*b*) T. Fleetham, J. Ecton, Z. Wang, N.Bakken and J. Li, *Adv. Mater.*, 2013, **25**, 2573.

8 (*a*) J. Kalinowski, M. Cocchi, D. Virgili, V. Fattori and J. A. G. Williams, *Adv. Mater.*, 2007, **19**, 4000; (*b*) X. Yang, Z. Wang, S. Madakuni, J. Li and G. E. Jabbour, *Adv. Mater.*, 2008, **20**, 2405; (*c*) L. Murphy, P. Brulatti, V. Fattori, M. Cocchi and J. A. G. Williams, *Chem. Commun.*, 2012, **48**, 5817.

9 (*a*) S. C. F. Kui, P. K. Chow, G. S. M. Tong, S.-L. Lai, G. Cheng, C.-C. Kwok, K.-H. Low, M. Y. Ko and C.-M. Che, *Chem. Eur. J.*, 2013, **19**, 69; (*b*) G. Li, T. Fleetham and J. Li, *Adv. Mater.*, 2014, **26**, 2931.

10 (a) C.-M. Che, S.-C. Chan, H.-F. Xiang, M. C. Chan, Y. Liu and Y. Wang, *Chem. Commun.*, 2004, 1484; (*b*) B.-P. Yang, C. C. C. Cheung, S. C. F. Kui, H.-F. Xiang, V. A. L. Roy, S.-J. Xu and C.-M. Che, *Adv. Mater.*, 2007, **19**, 3599; (*c*) G. Zhou, Q. Wang, X. Wang, C.-L. Ho, W.-Y. Wong, D. Ma, L. Wang and Z. Lin, *J. Mater. Chem.*, 2010, **20**, 7472.

11 (*a*) G. Schwartz, M. Pfeiffer, S. Reineke, K. Walzer and K. Leo, *Adv. Mater.*, 2007, **19**, 3672; (*b*) G. Schwartz, S. Reineke, K. Walzer and K. Leo, *Appl. Phys. Lett.*, 2008, **92**, 053311.

12 A. Poloek, C.-T. Chen, C.-T. Chen, *J. Mater. Chem. C*, 2014, **2**, 1376.

13 A. Poloek, C.-W. Lin, C.-T. Chen, C.-T. Chen, *J. Mater. Chem. C*, 2014, **2**, 10343.

14 S.-H. Liao, J.-R. Shiu, S.-W. Liu, S.-J. Yeh, Y.-H. Chen, C.-T. Chen, T. J. Chow and C.-I. Wu, *J. Am. Chem. Soc.*, 2009, **131**, 763.

15 J. Brooks, Y. Babayan, S. Lamansky, P. I. Djurovich, I. Tsyba, R. Bau and M. E. Thompson, *Inorg. Chem.*, 2002, **41**, 3055.

16 Crystal data for **FPtdmaND**: $C_{21}H_{16}F_2N_4OPt$: *Fw* = 573.47, monoclinic, $P2_1/c$, Z = 4, *F*(000) = 1096. Cell dimendions: a = 12.2637(4) Å, b = 20.2483(7) Å, c = 6.9828(2) Å, $\alpha = 90^o$, $\beta = 92.168(2)^o$, $\gamma = 90^o$, V = 1732.72(10) Å^3, $2\vartheta_{max} = 50.0^o$, ρ_{cacld} = 2.198 mg m^{-3}. Of 48805 reflections, 3543 were

independence, 264 parameters, R (F_o) = 0.0197 (for reflections with $I > 2\sigma(I)$), R_w (F_o) = 0.0446 (for reflections with $I > 2\sigma(I)$). The GoF on F^2 was equal 1.099. Crystal data for **FPtpxzND**: $C_{32}H_{22}F_2N_4O_3Pt$: *Fw* = 743.62, triclinic, *P*-1, Z = 2, *F*(000) = 724. Cell dimendions: a = 7.1554(6) Å, b = 12.9732(12) Å, c = 14.4038(13) Å, α = 89.276(6)°, β = 82.908(5)°, γ = 74.477(5)°, V = 1278.2(2) Å^3, $2\vartheta_{max}$ = 50.0°, ρ_{cacld} = 1.932 mg m^{-3}. Of 57738 reflections, 5635 were independence, 382 parameters, R (F_o) = 0.0208 (for reflections with $I > 2\sigma(I)$), R_w (F_o) = 0.0422 (for reflections with $I > 2\sigma(I)$). The GoF on F^2 was equal 1.049. CCDC-1044625 and CCDC-1044626 contain the supplementary crystallographic data of **FPtdmaND** and **FPtpxzND**, respectively. These data can be obtained free of charge via www.ccd.cam.ac.uk/conts/retrieving.html (or from the Cambridge Crystallographic Data Centre, 12, Union Road, Cambridge CB21EZ, UK; fax: (+44)1223-336-033; or deposit@ccdc.cam.ac.uk).

17 (*a*) L. Chassot, E. Muller and A. V. Zelewsky, *Inorg. Chem*., 1984, **23**, 4249; (*b*) S.-W. Lai, M. C.-W. Chan, T.-C. Cheung, S.-M. Peng and C.-M. Che*, Inorg, Chem*., 1999, **38**, 4046; (*c*) S.-Y. Chang, J.-L. Chen, Y. Chi, Y.M. Cheng, G.-H. Lee, C.-M. Jiang and P.-T. Chou, *Inorg. Chem*., 2007, **46**, 11202.

18 (*a*) B. Yin, F. Niemeyer, J. A. G. Williams, J. Jiang, A. Boucekkine, L. Toupet, H. L. Bozec and V. Guerchais, *Inorg. Chem*., 2006, **45**, 8584; (*b*) Z. M. Hudson, C. Sun, M. G. Helander, H. Amarne, Z.-H. Lu and S. Wang, *Adv. Funct. Mater*., 2010, **20**, 3426.

19 (*a*) K. M.-C. Wong and V. W.-W. Yam, *Acc. Chem. Res.*, 2011, **44**, 424; (*b*) E. Rossi, A. Colombo, C. Dragonetti, D. Roberto, F. Demartin, M. Cocchi, P. Brulatti, V. Fattorie and J. A. G. Williams, *Chem. Commun*., 2012, **48**, 3182; (*c*) P. Brulatti, V. Fattori, S. Muzzioli, S. Stagni, P. P. Mazzeo, D. Braga, L. Maini, S. Militae and M. Cocchi, *J. Mater. Chem*. *C*, 2013, **1**, 1823; (*d*) L.-M. Huang, G.-M. Tu, Y. Chi, W.-Y. Hung, Y.-C. Song, M.-R. Tseng, P.-T. Chou, G.-H. Lee, K.-T. Wong, S.-H. Cheng and W.-S. Tsai, ***J. Mater. Chem. C,*** 2013, **1**, 7582.

20 (*a*) D. S. Tyson, J. Bialecki, F. N. Castellano, *Chem. Commun.*, 2000, 2355; (*b*) D. S. Tyson, K. B. Henbest, J. Bialecki and F. N. Castellano, *J. Phys. Chem. A*, 2001, **105**, 8154; (*c*) B. Maubert, N. D. Mcclenaghan, M. T. Indelli and S. Campagna, *J. Phys. Chem. A*, 2003, **107**, 447; (*d*) S. Ji, W. Wu, W. Wu, P. Song, K. Han, Z. Wang, S. Liu, H. Guo and J. Zhao, *J. Mater. Chem.*, 2010, **20**, 1953.

21 G. Schwartz, S. Reineke, T. C. Rosenow, K. Walzer and K. Leo, *Adv. Funct. Mater.*, 2009, **19**, 1319.

22 X.-H. Zhu, J. Peng, Y. Cao and J. Roncali, *Chem. Soc. Rev*., 2011, **40**, 3509.

23 M. S. Lowry, W. R. Hudson, R. A. Pascal and Jr, S. Bernhard, *J. Am. Chem. Soc*., 2004, **126**, 14129.

24 J. C. de Mello, H. F. Wittmann and R. H. Friend, *Adv. Mater.*, 1997, **9**, 230.

25 C.-L. Chiang, M.-F. Wu, D.-C. Dai, Y.-S. Wen, J.-K. Wang and C.-T. Chen, *Adv. Funct. Mater*., 2005, **15**, 231.

26 M. Thelakkat and H.-W. Schmidt, *Adv. Mater*., 1998, **10**, 219.

27 G. M. Sheldrick, *SHELXL-97*, University of Gottingen, Germany, 1997.

28 L. J. Farrugia, *J. Appl. Cryst*., 1999, **32**, 837.

29 S. R. Forrest, D.D.C. Bradley and M. E. Thompson, *Adv. Mater*., 2003, **15**, 1043.

30 B. E. Koene, D. E. Loy and M. E. Thompson, *Chem. Mater*., 1998, **10**, 2235.

31 P. J. Low, M. A. J. Paterson, D. S. Yufit, J. A. K. Howard, J. C. Cherryman, D. R. Tackley, R. Brookc and B. Brown, *J. Mater. Chem*., 2005, **15**, 2304.

32 J. Shi, C. W. Tang and C.H. Chen, *U.S. Pat*. No. 5645948, 1997.

33 Y. You and S. Y. Park, *J. Am. Chem. Soc*., 2005, **127**, 12438.

34 D. Kourkoulos, C. Karakus, D. Hertel, R. Alle, S. Schmeding, J. Hummel, N. Risch, E. Holder and K. Meerholz, *Dalton Trans*., 2013, **42**, 13612.

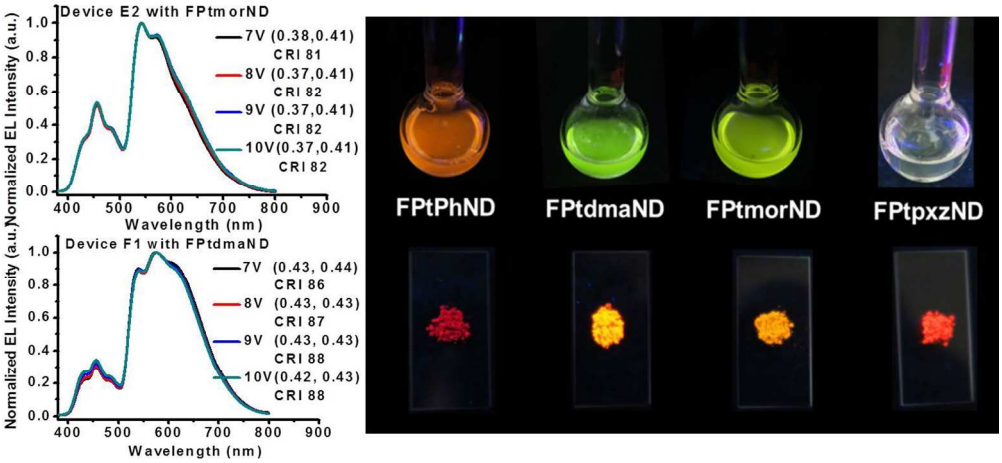

258x119mm (150 x 150 DPI)